Bioseco Pilot Study Results Report

Camera-Based Anti-Collision System

Species Protection Assessment

Esther Clausen

Dr. Jorg Welcker

Dr. Thilo Liesenjohann

Husum, November 2023

THIS DOCUMENT IS TRANSLATED FROM GERMAN BY PROFESSIONAL TRANSLATOR ON ORDER OF BIOSECO S.A.

BIOCONSULT SH NOR THE AUTHORS ASSUME NO RESPONSIBILITY FOR ANY DEVIATIONS FROM THE ORIGINAL.

Project name	Project name Bioseco Pilot Study – Species Protection Assessment	
Project number	21_1176	
Contractor		BioConsult SH GmbH & Co.KG Schobüller Str. 36 D - 25813 Husum Phone: +49 (0)4841 77937-10 www.bioconsult-sh.de
Project management	Esther Clausen	██████████████████
Deputy project management	Dr. Thilo Liesenjohann	██████████████████
Report preparation	Esther Clausen	
Checked/approved	On July 04, 2023	Version: June 13, 2023
	Jorg Wecker	j██████████████
Cover image	Bioseco system at the WT (BioConsult SH 2021)	
Suggested citation	Bioseco Pilot Study Results Report – Camera-Based Anti-Collision System – Species Protection Assessment BioConsult SH (2023): Bioseco Pilot Study Results Report – Camera-Based Anti-Collision System – Species Protection Assessment, BioConsult SH, Husum. Research reports: cite with authors Clausen, E. (2023): Bioseco Pilot Study Results Report – Camera-Based Anti-Collision System – Species Protection Assessment BioConsult SH, Husum.	
Employer	PNE AG Peter Heinlein-Str. 2-4 27472 Cuxhaven	
Employer's contact person	Jannes Kreutzfeldt	██████████████████

Table of contents

List of figures

List of tables

List of abbreviations and technical terms

ACS	Anti-collision system
Azimuth	Used with the laser rangefinder; a horizontal angle oriented according to a cardinal direction
BNatSchG	Federal Nature Conservation Act
BVerwG	Federal Administrative Court
Detection rate	Rate at which target bird species are actually detected as targets by the ACS
Recognition rate	Rate at which detected target species are correctly classified by the ACS according to their size
Flight	Flight of an individual
Flight corridor	Area regularly flown through/over by a species/breeding pair between breeding site and foraging area; result of habitat potential analysis, if applicable
Flight sequence	(Up to) five-minute interval of a flight
KNE	Competence Center for Nature Conservation and Energy Transition (Kompetenzzentrum Naturschutz und Energiewende)
LRF	Laser rangefinder; device for electro-optical distance measurement, here: Vectronix Vector 21 Aero model
Response range	Species-specific distance from the WT from which a shutdown must be initiated, here: red kite 378 m, white stork 512 m, and white-tailed eagle 529 m
Rotor area	Circular area swept by rotors
Rotor radius	Half of the rotor diameter of the planned WT type
Significance threshold	In species protection: procedure for assessing the risk of killing, here for wind-sensitive bird species
Spin mode	Slowing down the rotor speed of the WT
WT	Wind turbine(s)
WF	Wind farm
Target species	Red kite, white-tailed eagle, white stork

1   INTRODUCTION – GROUNDS AND OBJECTIVE

The expansion of wind turbines is increasingly in conflict with legal provisions for the protection of endangered bird species. As part of a pilot study on automatic bird detection and thus on demand-based wind turbine (WT) shutdown, a camera-based system from the manufacturer BIOSECO was tested on a Vestas V150 4.2 MW (total height 200 m, hub height 125 m, lower rotor passage 50 m). The BIOSECO anti-collision system (ACS) is intended to protect birds by reducing the significantly increased risk of killing bird species that are sensitive to wind power (here: red kite, white-tailed eagle and white stork) and thus preventing the occurrence of species protection prohibitions. The use of functional ACS aims to reduce the collision risks posed by turbine operation (rotor rotation). The collision mitigation effect is achieved by putting the turbine into spin mode.

This Results Report presents a species protection assessment of this system. This study focuses on the compliance with the species protection based on KNE specifications (see KNE Checklist 2021: BRUNS et al. 2021).

The performance features of the Bioseco system, such as detection rate, recognition rate, and coverage, were implemented and evaluated based on a professional trial (field test) in 2022. These system-specific performance features apply to sites with comparable visibility.

BIOCONSULT SH GMBH & CO. KG, Husum, was commissioned by PNE AG, Cuxhaven, to collect data and carry out a species protection assessment of the bird recognition system. For the data analysis part, BIONUM GMBH – Biostatistics and Ecological Statistics Office (Büro für Biostatistik und Ökologische Statistik) based in Hamburg was subcontracted.

1.1   Study area

The Vestas V150 4.2 MW WT with the installed Bioseco system is located in the wind priority area No. PR3_SEG_056 in the district of Segeberg and borders areas of the municipalities of Lentföhrden and Nützen. To the east runs the B4 federal highway in a north-south direction, which connects Hamburg with Bad Bramstedt. The area around the WT is also crisscrossed by smaller farm roads (see Fig. 1.1).

Grassland dominates the area west of the highway and occupies a large portion of the area. Arable land with cereals and maize crops can be found in the central area, but also scattered throughout the area. In the immediate vicinity of the WT, in addition to the agriculturally used areas, there are also grasslands, some of which are grazed by horses (see Fig. 1.3). To the east of the federal highway, there are succession areas of varying stages as a result of sand and gravel mining. To the north, there are settlement areas of the village of Lentföhrden.

To the northeast of the priority area and to the east of the federal highway, there are larger water bodies (including fishing lakes). The Krummbek runs north-south through the study area. In the southern area, there are larger, partly structurally rich forest areas with various tree species of different ages. To the west and east, there are smaller forest areas, some of which are artificially wooded, and smaller woodlands.

To the west of the priority area, at a distance of > 3 km, there is the Grotmoor, and to the south – the Nützener and Kaltenkirchener Heide (FFH area). The surrounding area of the WT is crisscrossed by linear structures such as kinks and kink remnants, field boundaries with and without copses, and copses with and without overhangs, especially to the west of the federal highway. Larger tree structures or other visual barriers are not located in the immediate vicinity of the WT, so that very good visibility conditions exist for the Bioseco system (cf. Fig. 1.2 to Fig. 1.4; see also sections 2.2 and 3.1).

Land use

Maize	
Field	
Field (fallow)	
Buckwheat, Phacelia	
Cereals	
Summer cereals	
Winter cereals	
Grassland (pasture)	
Grassland (pasture, permanently wet)	
Grassland (fallow)	

Grassland (meadow)	
Grassland (meadow, permanently wet)	
Grassland (solitary trees and shrubs)	
Succession areas	
Succession areas (woody vegetation)	
Forest (structurally rich)	
Forest (artificially wooded area)	
Water areas	
Settlement area	

Planned wind turbine (as of March 07, 2018)

500 m radius around planned WT

Priority area with the effect of suitable areas for wind energy use (Staatskanzlei SH, December 06, 2016)

1 km radius around priority area

Land use 2017

Project: 17_0557_a_Lentfoerden_WKN

Date: March 21, 2018

Editor: M. Defingou

Scale: 1:14.000

0   150   300   600 meter

N

Employer:
WKN AG
Otto-Hahn-Str. 12 - 16
25813 Husum

Contractor:
BioConsult SH GmbH & Co. KG
Schobüller Str. 36, 25813 Husum

Fig. 1.1: Land use in the WT area from 2017.

Fig. 1.2: Northwest view from the WT with the ACS installed (photo: BioConsult SH 2022).

Fig. 1.3: West view from the WT with the ACS installed (photo: BioConsult SH 2022).

Fig. 1.4: Southwest view from the WT with the ACS installed (photo: BioConsult SH 2022).

2 MATERIAL AND METHODS

2.1 Bioseco system "Long Range" mode of operation

A Bioseco "Long Range" detection module consists of a total of four camera sensors (13 Mpx), which are installed on a module both in the upper and lower area. The modules are installed directly on the wind turbine tower at a variable height of between 5 and 10 m and, if required for a specific project, also > 20 m, in the present case at a height of 7 m. To achieve a 360 degree monitoring area (see Fig. 2.2), a total of eight modules are installed on a WT, i.e. a total of 32 cameras per WT (see Fig. 2.3 and Fig. 2.4). Each of the Bioseco's eight installed detection modules monitors a section of 45° horizontal aperture angle totaling 360° (8 x 45°; see Fig. 2.5). This so-called stereo arrangement of the cameras makes it possible to determine the position (see section 2.6 and section 3.4).

All cameras combined have a vertical aperture angle of 65°. The elevation angle of the lower detection edge (slight inclination upwards) is 2° (see Fig. 2.1).

The relevant birds are detected from a distance of about 500 m and analyzed according to their size; no identification in terms of species is possible. Bioseco distinguishes five class sizes: extra small, small, medium, large and extra large. A signal to the WT to put it into spin mode occurs in this project for target species with a size ≥ medium. Species in this category include the red kite, white-tailed eagle and white stork. If a bird of category ≥ medium flies into the danger zone (see section 2.4 and section 2.5), the signal is sent to the WT in the future; in the present test procedure, a WT shutdown was only simulated. However, in determining the timely response of the WT, the signal chain was tested in real time. The Bioseco system additionally works with deterrence (light and sound), but this is not part of this study.
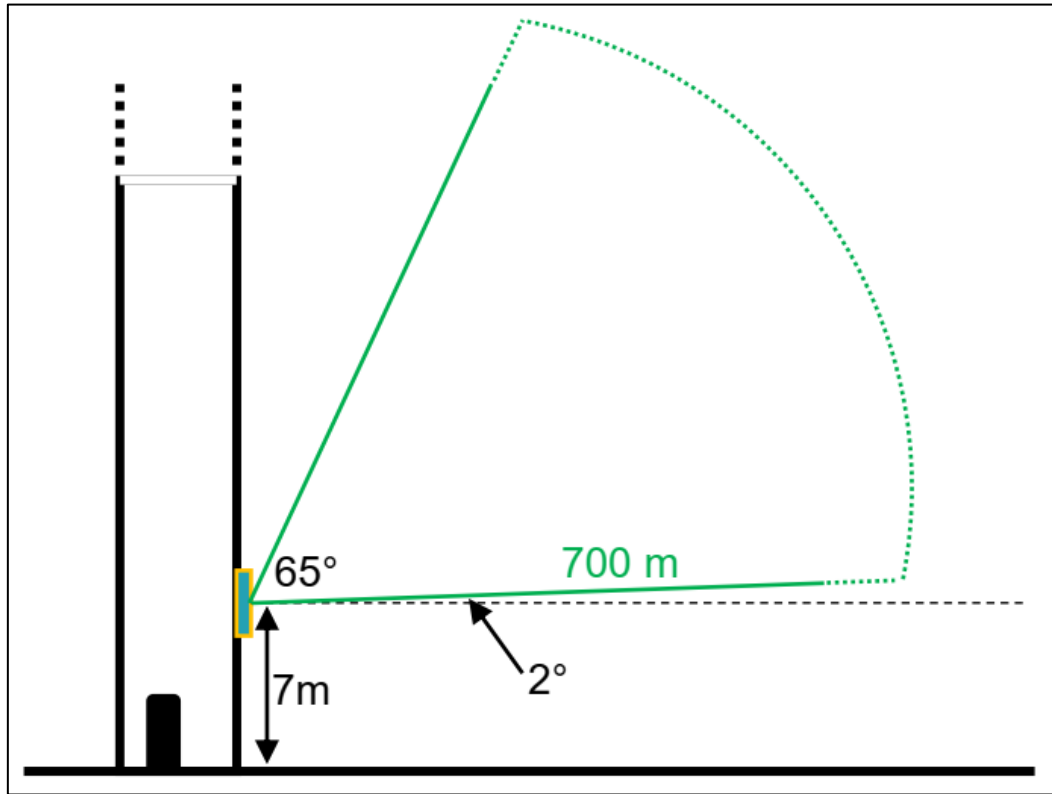
Fig. 2.1: Schematic representation of the camera features with indication of the installation height and the vertical aperture angle and the slight inclination upwards (representation unchanged PNE 2023).
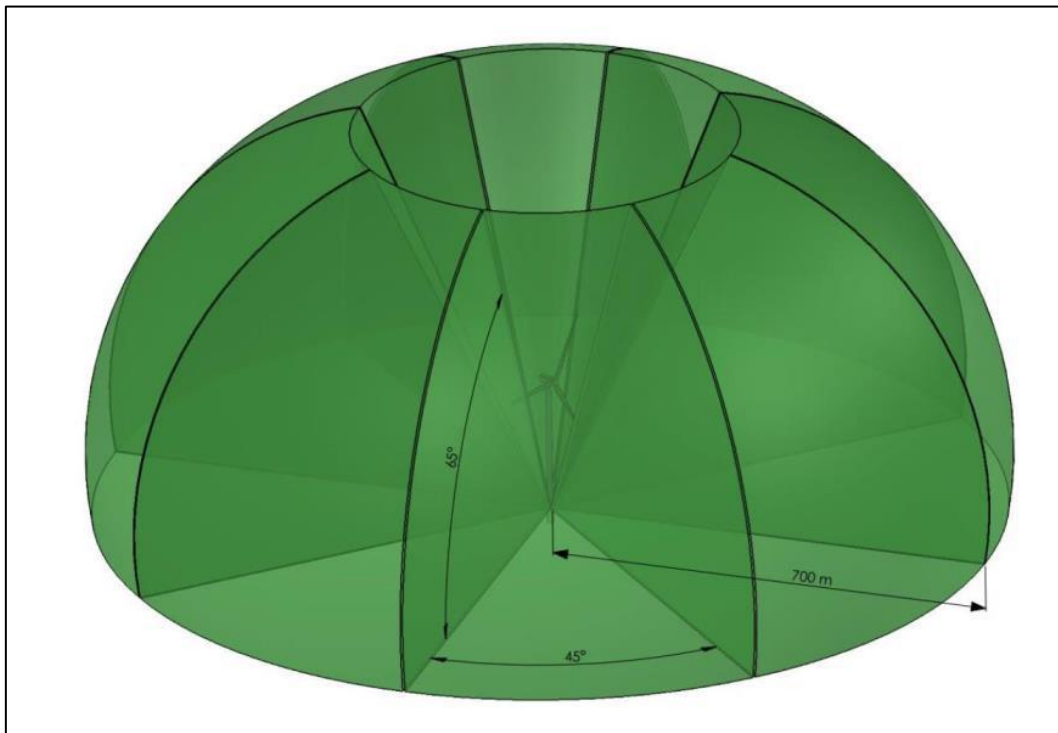
Fig. 2.2: Schematic 3D representation of the fields of view of the eight installed camera modules (representation unchanged Bioseco).

Fig. 2.3: The Vestas WT in Lentföhrden with eight Bioseco systems installed at a height of 7 m (photo: BioConsult SH 2022).

Fig. 2.4: Detailed view of the individual Bioseco detection modules (photo: BioConsult SH 2022).
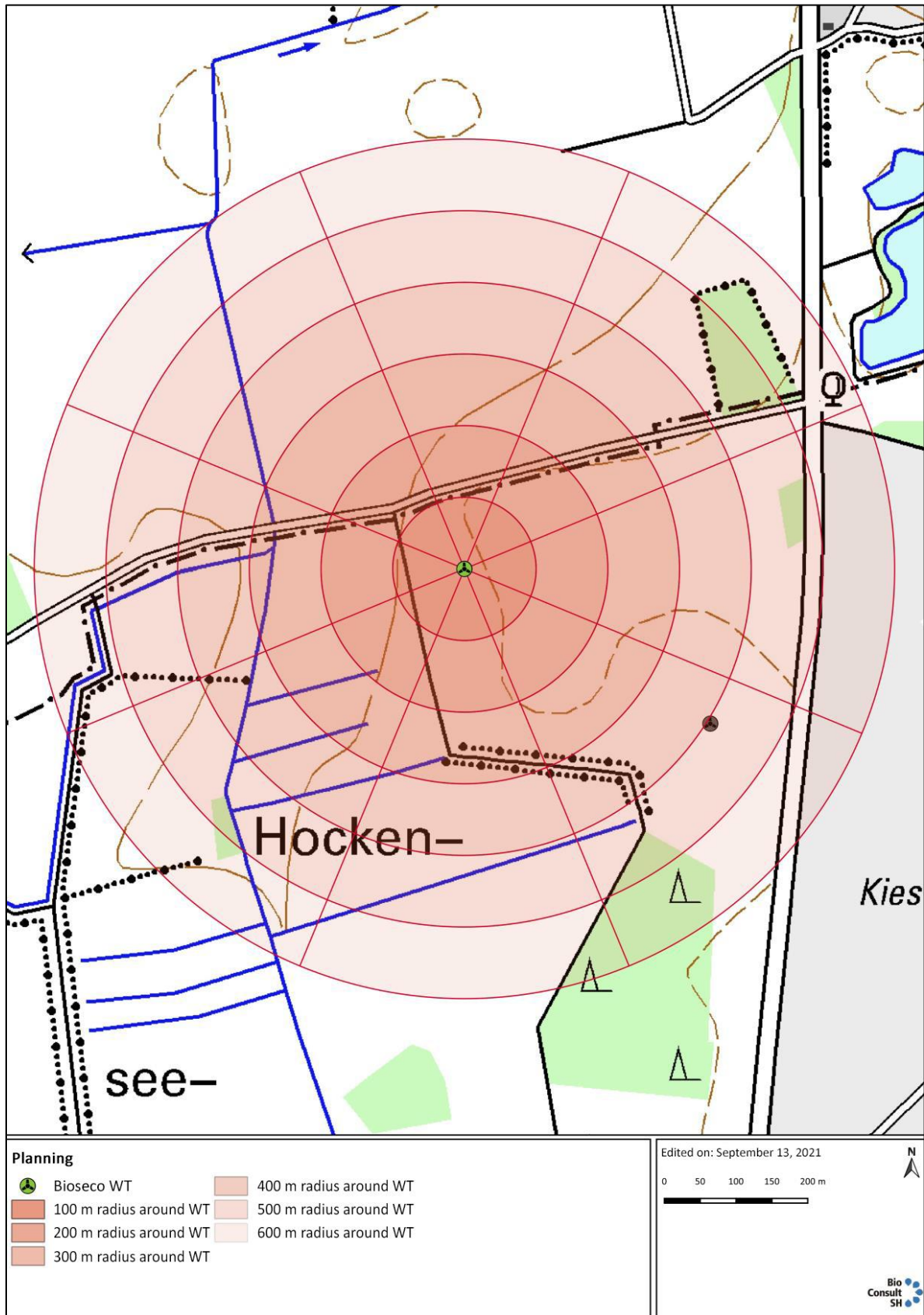
Fig. 2.5: *Detection range around the Vestas WT with the eight Bioseco systems (map prepared by BioConsult SH 2021).*

2.2 Bioseco system visibility and detection height

For the three target species (red kite, white-tailed eagle and white stork), the response ranges between 378 m and 530 m are decisive (see section 2.4); in addition, distances up to a maximum of 700 m (detection range) were evaluated.

For the present camera inclination angle of 2° and installation height of 7 m, the minimum detection height at the above three distances (378 m, 530 m and 700 m) was calculated by PNE (see section 3.1; J. KREUTZFELDT 2023). The evaluation of visibility and detection height of the Bioseco system was performed by PNE GmbH (J. KREUTZFELDT 2023). Digital surface models from the State Office for Surveying and Geoinformation (Landesamt für Vermessung und Geoinformation SH) with a resolution of less than 1 m in all three dimensions were used as the basis for the calculations, which were intersected with the camera aperture angles at the minimum detection height using GIS software.

2.3 Data basis

In order to validate the Bioseco system, reference data, through what the KNE calls a secondary system, are required. For this purpose, a *Vectronix Vector 21 Aero* laser rangefinder (LRF) was used (see Fig. 2.6). The suitability of this device for this type of survey has been proven in various projects and BioConsult SH has many years of experience in surveying and measuring different bird species and issues. The device has been successfully used for distance and flight altitude determination of birds in several countries (PENNYCUICK et al. 2013; ASCHWANDEN et al. 2015; SKOV et al. 2015, 2018; JENSEN et al. 2016). The target species studied here (red kite, white-tailed eagle and white stork) can be tracked and surveyed well with the LRF because of their size and relatively quiet flight behavior.

Fig. 2.6: LRF from Vectronix Vector 21 Aero model.

Technical data of the Vectronix Vector 21 Aero LRF:

- 42 mm binocular with 7x magnification, adjustable eye relief, distance measurement up to 12,000 m with an accuracy of less than 5 m,

- a class 1 laser is used (DIN EN 60825-1: the emitted laser radiation is not dangerous or the laser is in a closed housing),

- dimensions: 205 mm x 178 mm x 82 mm, weight: 1.7 kg,

- powered by a 6 V lithium battery or external power source from 7 V DC to 14 V DC,

- Bluetooth or RS-232 interface to PC, smartphone, tablet or Garmin 60/72/76 GPS.

Ideal conditions:

- clear atmosphere, cloudy sky, dawn/dusk,

- good reflectivity of the target object,

- rough surface of the target object perpendicular to the laser beam,

- stable point of view (to make sure that the laser beam does not lose the target object) – for this purpose a tripod was used.

Unfavorable conditions:

- snowfall, fog, rain, haze, high humidity, heat,

- small target objects that do not "hold" and reflect the entire laser beam,

- "difficult" target objects (dark, uneven).

Since a magnetic compass is built into the LRF, problems may occur in the vicinity of metal objects (so-called declination). To compensate for potential declination, the LRF was calibrated and adjusted to the WT prior to each session.

The ornithologist operates the LRF and pays attention to the concrete target data collection of the passing birds (focus on the red kite, white-tailed eagle, white stork; but all large birds and birds of prey are surveyed) and documents all observations, additionally handwritten with the respective species identification. Since Bioseco does not use species recognition, species identification based on size class is evaluated using these data. If possible, the target species should be surveyed as frequently as possible. Here, all three target species fall into the ≥ medium category.

In general, the handling of the LRF is comparable to that of binoculars. However, the LRF is additionally equipped with a battery-powered laser system that can be used to determine the distance, height and, if necessary, direction of an object. With known geographic position and altitude of the observer, the use of the LRF can provide three-dimensional data from the birds surveyed. In this case, the LRF is usually operated at a frequency of about 10 second intervals and the position and elevation data are automatically stored via GPS/smartphone/laptop etc. (Skov et al. 2015). In this way, longer series of data records of individual birds or groups of birds can be created.

For the electronic storage and display of the measurement data, the LRF can be coupled with various end devices; in the present test setup, the LRF was coupled and operated with a GARMIN GPS.

The Bioseco system generates position data from the detected objects approximately every 100 ms. To validate the Bioseco system, birds were surveyed in parallel to the Bioseco system by at least one ornithologist (BioConsult SH, see Fig. 2.7) using an LRF on 34 detection days (see section 2.4.1.). Each

of these so-called tracks consists of LRF samples, which are recorded approx. every 5 to 10 seconds. Based on these data, the ACS detection rate is determined by the Bionum office (see section 3.1). A comparison of the LRF data with the generated log files of the Bioseco cameras is performed. The ornithologist uses the LRF to measure radial distance, pitch angle, and azimuth using a laser beam on the measured target object. From these parameters, the LRF measures the height of the target object. The ornithologist's position is determined using a GPS smartphone, and multiple measurements of the target object create a three-dimensional flight track. For each LRF track, the species was additionally determined and logged by the ornithologist and compared with the camera log files.

Fig. 2.7: Parallel detection with the LRF by BioConsult SH (photo: PNE 2022).

A wide variety of data was collected in the WT area as part of the study, making it possible to assess the performance of the system. The data collected include:

- spatiotemporal LRF data of approaching target species (collected by BioConsult SH in 2022),

- spatiotemporal camera-based data of approaching target species from the ACS,

- spatiotemporal GPS data from targeted drone flights,

- signal transmission times and stop times from the ACS and WT (PNE 2023).

For the purposes of this report, these data will be used to examine the performance of the system in light of the KNE Checklist (BRUNS et al. 2021). Here, the following points, among others, are analyzed:

- the definition of meaningful target species-specific detection and response ranges;

- the target species-specific detection rate (i.e., the rate at which target bird species are actually detected as targets by the ACS);

- the target species-specific recognition rate (i.e., the rate at which detected target species are correctly classified by the ACS according to their size);

- the position accuracy of the ACS-based measurements;

- the timely response of the WT shutdown including the stop time of the WT.

Data manipulations were excluded by first sending the ACS data from Bioseco to BioConsult SH and subsequently providing the LRF data by BioConsult SH.

Table 2.1   *Detection sessions in the period from March 09, 2022 to September 22, 2022 with indication of observation duration and number of detectors.*

No.	Date	Number of detectors	Period	Duration [hh:mm]
1	March 09, 2022	1	09:00 – 17:00	08:00
2	April 12, 2022	1	09:30 – 17:30	08:00
3	April 16, 2022	1	09:00 – 17:00	08:00
4	April 22, 2022	2	10:00 – 18:00	16:00
5	April 26, 2022	1	07:00 – 15:00	08:00
6	April 28, 2022	1	07:30 – 15:30	08:00
7	April 29, 2022	1	06:30 – 14:30	08:00
8	May 03, 2022	2	07:00 – 15:00	16:00
9	May 05, 2022	2	07:30 – 15:30	16:00
10	May 23, 2022	1	08:00 – 16:00	08:00
11	May 24, 2022	2	08:00 – 18:00	16:00
12	June 15, 2022	1	06:00 – 14:00	08:00
13	June 22, 2022	2	08:00 – 16:00	16:00
14	June 23, 2022	2	07:00 – 15:00	16:00
15	June 29, 2022	2	07:00 – 15:00	16:00
16	July 05, 2022	2	07:00 – 15:00	16:00
17	July 12, 2022	2	07:00 – 15:00	16:00
18	July 13, 2022	2	07:30 – 15:00	16:00
19	July 28, 2022	2	08:00 – 16:00	16:00
20	August 19, 2022	2	07:00 – 15:00	16:00
21	August 23, 2022	2	07:30 – 15:30	16:00
22	August 25, 2022	1	07:00 – 15:00	08:00
23	August 26, 2022	1	08:00 – 16:00	08:00
24	August 29, 2022	1	08:00 – 16:00	08:00
25	August 30, 2022	1	09:00 – 17:00	08:00
26	August 31, 2022	1	04:30 – 12:30	08:00
27	September 02, 2022	1	08:00 – 16:00	08:00
28	September 04, 2022	1	10:00 – 18:00	08:00
29	September 05, 2022	1	04:30 – 12:30	08:00
30	September 07, 2022	1	08:30 – 16:30	08:00
31	September 08, 2022	1	04:30 – 12:30	08:00
32	September 12, 2022	1	08:00 – 16:00	08:00
33	September 21, 2022	1	06:30 – 14:30	08:00
34	September 22, 2022	1	05:00 – 13:00	08:00

2.4 Response range and detection range

The data of detection range and response distance is based on the measurements/validations of case studies presented below. However, these values should be plausibly derived beforehand. The detection rate calculations or evaluations were carried out by the Bionum office

The **response range** here is derived from the distance a specific bird species travels within the time it takes to initiate a shutdown signal and transition of the WT into spin mode. The time required to put the wind turbine into spin mode is given as 26 s on average. Additionally, the addition of the time delay due to the WT (t_latency = 7 seconds) has to be added. In many respects, this approach represents an estimation in the sense of precaution, because

- it is assumed that the bird flies directly towards the risk area (and does not tangentially intersect the response range);

- real flight speeds were used, i.e. it was assumed for the calculation of the response distance that the bird flies in a straight line (which is often not the case – e.g. during search flight or thermal circling, which may significantly reduce the effective speed);

- uncertainties from the position accuracy were added to the response range; ergo, it was assumed that the error is always in favor of an overestimated distance; and

- the rotor blade length was added to the response range, which assumes the worst case (and most unlikely) scenario that the bird flies exactly within the rotor blade disc path.

Regarding the mean flight speeds, we averaged all available values from the literature and used them to follow a maximally objective path. With regard to the red kite, there are the data of 7.9 m/s (Spröttge/planungsgruppe grün GmbH, p. 31 in (BRUNS, E. ET AL 2019); 9.2 m/s (TENNEKES 1997); 10.1 m/s (BRUDERER & BOLDT 2001); 7.9 m/s and 10.9 m/s, respectively (PENNYCUICK 2001); 5.1 m/s (FRÜH & STARK 2020); 8.5 m/s (SPAAR 1997); and 8.3 (MERCKER et al. 2023). This resulted in a mean value of **8.14 m/s**, which was assumed for the **red kite** in the following. Regarding the **white stork**, there were three different calculations in BRUDERER & BOLDT 2001, which refer to different behaviors and measurement methods, namely 13.5 m/s; m/s as well as 12.9 m/s. The mean value is **11.83 m/s**. Finally, for the **white-tailed eagle**, 13.1 m/s were calculated in(BRUDERER & BOLDT 2001), and 11.2 m/s and 12.6 m/s, respectively, in(PENNYCUICK 2001). Here, the mean value is thus **12.3 m/s**.

The time required to initiate a shutdown signal and put the WT into spin mode was studied separately for the specific WT sampled (Vestas V150 4.2 MW) as part of the PNE project being evaluated. For this purpose, 92 stops were actively performed with a drone and then it was determined how long the different steps took to achieve spin mode. An overview of the steps up to the point where the stop signal was sent to the WT is given in Fig. 2.8. This showed that the mean delay was 7 seconds (minimum: 1 second, maximum: 11 seconds), which was largely due to the fact that other signals have a higher priority in the context of farm control. To these 7 seconds of latency, the mean time it takes for a turbine to go from run to spin mode must be added. This value was also determined empirically based on 11 initiated stops and is on average 26 seconds (minimum: 22 seconds, maximum: 32 seconds).

The response radius, $r_{Response}$, is finally given by the formula

$$r_{Response} = \left(V_{Bird} \cdot \left(t_{Stop} + t_{Latency} \right) + r_{Rotor} \right) \cdot f_{RDE},$$

where V_{Bird} denotes the species-specific flight speed (see above), t_{Stop}= 26 sec the time to go from run to spin mode, $t_{Latency}$ = 7 sec the latency, r_{Rotor} = 75 m the rotor blade length, and f_{RDE} the relative local measurement error.
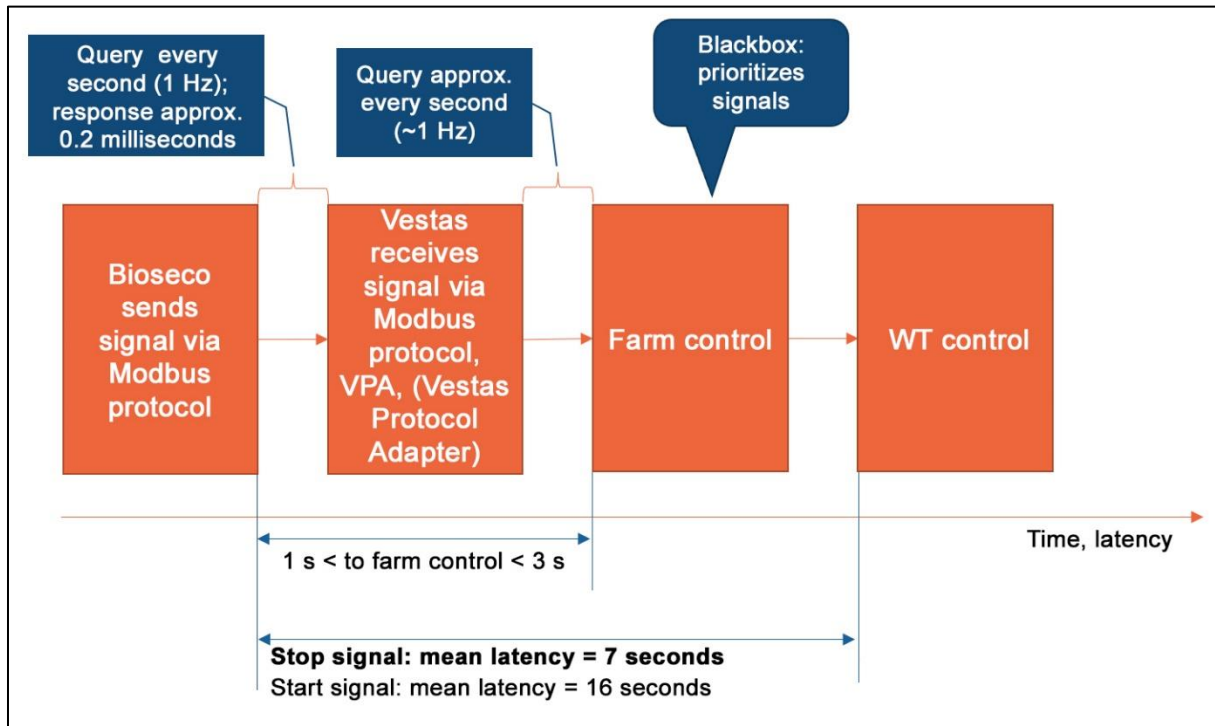
Fig. 2.8: The different steps from sending the Bioseco stop signal to the arrival of this signal at the WT.

Thus, taken together, the following **response ranges** are obtained for the bird species considered:

In addition, it should be noted that the response radii calculated above are also unnecessarily increased by the ACS-independent fact that signal prioritization in the context of wind farm control results in a high value of $t_{Latency}$.

According to the KNE Checklist, the **detection range** should at least correspond to the response radius; a distance of 500 m is recommended as a orientation value for the minimum range. In the course of the present analyses, therefore, the three different distances of **378 m, 530 m** and **700 m** are analyzed with respect to the detection and recognition rate. In addition, the continuous change of both rates from 0–700 m is presented, which allows an even more differentiated view.

It is crucial that the detection range is larger than the response range, so in this case for the white stork and white-tailed eagle, the evaluations are considered to have a radius of **530 m**, instead of 512 m and 529 m, respectively.

Red kite: $r_{Response}$ = 377.98 m

White stork: $r_{Response}$ = 511.93 m

White-tailed eagle: $r_{Response}$ = 528.99 m

2.4.1 Field tests

The concept for studying the detection rate is based on the comparison of birds recorded in the field (locally and temporally located) by ornithologists (BioConsult SH, 2021, see section 2.3) with what was recorded by the ACS. Specifically, observers used laser rangefinders (LRF), which can provide relatively precise location of birds (Ransom, D., & Pinchak, W. E. 2003). For this reason, it is assumed in the following (simplified) that the LRF data are in principle not subject to any significant local and/or temporal error (see also section 2.3).

In total, LRF data from 34 study days (March 09, 2022–September 22, 2022, see Table 2.1) were used. Due to problems with the LRF timestamp, 2 days were previously removed from the analyses. Each LRF track often consists of multiple recorded points associated with an individual bird. LRF points were preselected in such a way that LRF points were a priori excluded from the analyses if they either exceeded the detection range under consideration or fell below the minimum detection level. The latter is reflected in the section "Spatial coverage at the site" (see sections 1.1 and 3.1).

The mapping between LRF points and ACS points (the latter having a temporal resolution of about 0.1 seconds) was done by a two-step procedure: in a first step, the ACS data were spatiotemporally constrained to the area of the LRF point. For this purpose, those ACS data were selected which, in terms of time, were +/- 10 seconds around the respective LRF time stamp considered, as well as in a radius corresponding to 0.4 times the distance between WT and LRF point. If, for example, an LRF point is located 100 m away from the WT, all ACS points closer than 40 m to the LRF point are taken into account. Both limit values (+/- 10 seconds and R=0.4) were determined empirically and plausibility checked based on multiple reviews of individual tracks. In a second step, the one that showed the shortest 3D distance to the ACS point was selected from the set of all remaining ACS points. If no ACS point was located within the above-mentioned spatiotemporal buffer, the LRF point was evaluated as "not recorded".

2.4.2 Statistical evaluation

The data to be analyzed is a binary variable that classifies between "recorded" and "not recorded". In the simplest case, mean values of the corresponding rates can simply be determined here. However, the variable is not normally distributed, so techniques that do not assume a normal distribution must be used to calculate the variance (e.g. to obtain confidence intervals) (Field, A., Miles, J., & Field, Z.

2012). For the present analyses, we used so-called bootstrap methods (CARPENTER, J., & BITHELL, J. 2000; CANTY, A. J., DAVIDSON, A. C., HINKLEY, D. V., & VENTURA, V. 2006 for this purpose, each based on N=2000 resamples. We have referred to this approach as "simple" in the following.

In fact, however, the statistical situation is somewhat more complex, because time series are examined, whereby additionally the LRF points are to be assigned to single individuals, so that in several respects a problem of "pseudo-replication" exists (HURLBERT, S. H. 1984), which can lead to a (possibly clear) underestimation of confidence intervals as well as to biased determined rates. For this reason, we applied a second analysis strategy that adequately addresses this data situation. In particular, the analysis here was carried out using appropriate regression methods, the "logistic regression methods", which belong to the "generalized linear models" (GLMs) (ZUUR, A., IENO, E., & SMITH, G. M. 2007; BOLKER et al. 2009; FIELD, A., MILES, J., & FIELD, Z. 2012). Membership in different individuals was included here by using the track ID as a "random intercept" in the context of "mixed modeling," resulting in the class of "generalized linear mixed models" (PINHEIRO, J. C., & BATES, D. M. 2000; BOLKER et al. 2009; ZUUR et al. 2009). In addition, temporal autocorrelation was analyzed using pACF plots and integrated as a suitable autoregression structure (AR1) (ZUUR, A., IENO, E., & SMITH, G. M. 2007; ZUUR et al. 2009; KORNER-NIEVERGELT, F., ROTH, T., VON FELTEN, S., GUELAT, J., ALMASI, B., & KORNER-NIE- VERGELT, P. 2015). We have referred to this approach as "GLMM" in the following.

By its nature, the complex method leads on the one hand to more realistic (and larger) confidence intervals, since temporal autocorrelation is taken into account, and on the other hand to somewhat lower estimated rates. The latter is due to the fact that, in an evaluation at LRF point level, those tracks for which there are a particularly large number of measured LRF points are particularly strongly included in the analysis. These are then possibly again the flights which could be recorded particularly well by the observed persons but also by the ACS. However, the use of the track ID as a "random intercept" (see above) leads to the fact that the data are not evaluated point- but rather individual-specific, which corrects the distorting effect mentioned above.

Finally, for the analysis of rates as a function of distance between LRF target and ACS, distance was used as a potentially nonlinear predictor (using regression splines), which then resulted in "generalized additive mixed models" (GAMMs) (HASTIE, T., & TIBSHIRANI, R. J. 1990; ZUUR, A. F. 2012; WOOD 2017). Otherwise, these models were structurally similar to the GLMMs mentioned above.

2.5   Size classification

The calculations and evaluations for the size classification were carried out by the Bionum office.

2.5.1   Field tests

The Bioseco system does not work with species identification, but with size classification of the birds. Bird size is recorded by wingspan and divided into five different classes: *extra small, small, medium,*

large and *extra large*. All birds defined as *extra small* are filtered out in advance by Bioseco. The birds determined as *small* have a wingspan of 0.7 m to 1.2 m.

Shutdowns by the Bioseco system would only occur if there was a classification >= "medium", i.e., all birds that have a wingspan greater than 1.2 m. In the present test run, the WT was not shut down in real, it was only indicated on the web interface of Bioseco at which time the WT would have gone into spin mode. Accordingly, each of the three target species treated was classified as "correctly classified" if the bird size determined by the ACS was "medium," "large," or "extra large." The analyses were based on all LRF points that were evaluated as "recorded" (cf. previous section).

2.5.2   Statistical evaluation

Again, this is a binomial variable to be examined (analogous to the situation in the context of the detection rate) with the levels "correctly classified" vs. "incorrectly classified" (hereafter referred to as the recognition rate); accordingly, the statistical analysis can be performed quite analogously to that in the context of the detection rate.

2.5.3   Correction of the recognition rate/size classification

The ACS data for analyzing the recognition rate contained a fundamental problem: each track segment which had been assigned its own track ID by the ACS was overwritten with the classification determined by the ACS for the last data point (i.e. with the greatest certainty) before the data was saved and forwarded. After consultation with PNE, it was not possible to acquire the original/point-specific classifications that were actually necessary for the analysis of the recognition rate. The analyzed detection rates would thus be estimated too optimistically, as the classifications of uncertain points would be overwritten by more certain classifications.

Thus, the following additional correction step, discussed and developed together with PNE, was taken in order to make it possible to estimate the detection rate:

In the first step, PNE carried out a manual redetermination of the LRF tracks for the ACS data. In particular, the stop signal of the ACS and the current distance between the ACS and the target were determined for each LRF track in the Bioseco web application. This made it possible to reconstruct the percentage of the LRF tracks that were finally classified when the reaction radius was exceeded. Here, the reaction radius was 283 m in one part of the data, which was changed to 407 m later on. In the second step, a straight line through the two percentage points was used to extrapolate/interpolate for each species complex (red kite vs. white-tailed eagle + white stork) the percentage of the LRF tracks that were correctly classified at a specific distance. For distances below the value at which the straight line intersected 0%, it was assumed that no correction was necessary. For the red kite, this resulted in a correction factor for the detection rate of y%=0.0007*distance-0.0977 (N=42 LRF tracks), while for the white-tailed eagle + white stork (which, due to the similar size, were evaluated together) of y%=0.0012*distance-0.326 (N=47 LRF tracks).

The difference in the uncorrected vs. corrected detection rate as a function of is shown graphically for the individual species in Appendix 2. However, the correction of the determined detection rates for

different reaction radii (see Section 3.3 and Appendix A2) is somewhat more complex, as each circular area contains points at various distances from the ACS. The corresponding correction values were determined numerically by dividing a corresponding virtual circular area into 10,000 elements for each reaction radius R under consideration, then calculating the distance to the center point for each of these elements and determining the correction factor. Then, the final correction factor was calculated from the average of 10,000 values.

The correction described in this section is not optimal from a statistical point of view, partly because the uncertainties introduced into the system by the correction are not reflected in the calculated confidence intervals and the latter can therefore be (under certain conditions significantly) underestimated. In our view, however, this is currently the only possible way of estimating detection rates and we consider the estimated figures to be generally realistic. Nevertheless, for future analyses, it would be essential to work with data that indicates the classification available for each ACS data point at that specific time.

2.6 Position accuracy

The calculations and evaluations for the position accuracy were carried out by the Bionum office (BIONUM GMBH 2023). The position accuracy of the ACS was evaluated using three drone flights. The GPS reference used is the GPS Standard Positioning Service (GPS ACCURACY n.d.), which achieves a horizontal accuracy of 7 m in 95% of the measurements.

From the measurement points of the drone GPS with a resolution of 1 Hz, those points are determined according to the reference object method that are detected by the ACS ($\Delta t = \pm 1$ s, alpha = 0.4). Reference object method means the following, the ACS generates position data from the detected objects approx. every 100 ms. For the verification of the Bioseco system, reference objects were used for comparison. These reference objects are birds located by ornithologists using LRF approx. every 5 to 10 seconds. The challenge is to filter out the reference objects in the multitude of automatically detected objects from the ACS, since each LRF has deviations in position and time compared to the ACS and vice versa.

Then, the spatially closest ACS measurement point is selected from the above data set to the respective drone measurement point. A relative distance error (RDE) from the selected ACS measurement point is calculated. RDE describes the ratio of the distance from the drone and the ACS measuring point to the WT $RDE = \frac{|distance_{ACS} - distance_{drone}|}{distance_{drone}}$ e. g. RDE = | (80 m - 100 m) | / 100 m = 0.2 → RDE of 20%. The individual measurement points are sorted into distance classes from 0–800 m in 50 m increments and the median and mean RDE per distance class are determined in each case.

Fig. 2.9: Drones used for position accuracy determination, wingspan of 1.5 m and 2 m (photo: PNE 2023).

The latter was also quantified in separate experiments in which three different drone flights (with two different maximum diameters: 1.5 m and 2.0 m) were specifically performed, and then the GPS positions of the drone were matched with the ACS-averaged positions (cf. Fig. 3.12 – center/top). In particular, the closest ACS point in time and location was assigned to each drone GPS point – analogous to the procedure for determining recognition and detection rates (see above). Drone GPS points without assignable ACS points were removed from the analysis as this issue is already reflected in the detection rate. The final number of data points used were N=2,317, N= 1,295 and N=1,599.

3   RESULTS

3.1   Visibility and detection height

Visibility was calculated for the 378 m, 530 m and 700 m response ranges, as shown in section 2.2. The minimum detection height at the above three distances, at an installation height of 7 m and a camera inclination angle of 2 degrees, was calculated. At a distance of 700 m, the minimum detection height was 32 m. At a distance of 530 m, the cameras achieved a minimum detection height of 26 m; at a distance of 378 m, this was 20 m. All heights refer to the height of the ground or foundation from the WT tower (see Fig. 3.1 and Fig. 3.2).

The lowest detection height at different distances:

Radius of 378 m (see Fig. 3.3)**:**

- tan(2°)*378 m + 7 m = **20.2 m** (rounded to 20 m)

Radius of 530 m (see Fig. 3.4)**:**

- tan(2°)*530 m + 7 m = **25.5 m** (rounded to 26 m)

Radius of 700 m (see Fig. 3.5):

- tan(2°)*700 m + 7 m = **31.4 m** (rounded to 32 m)
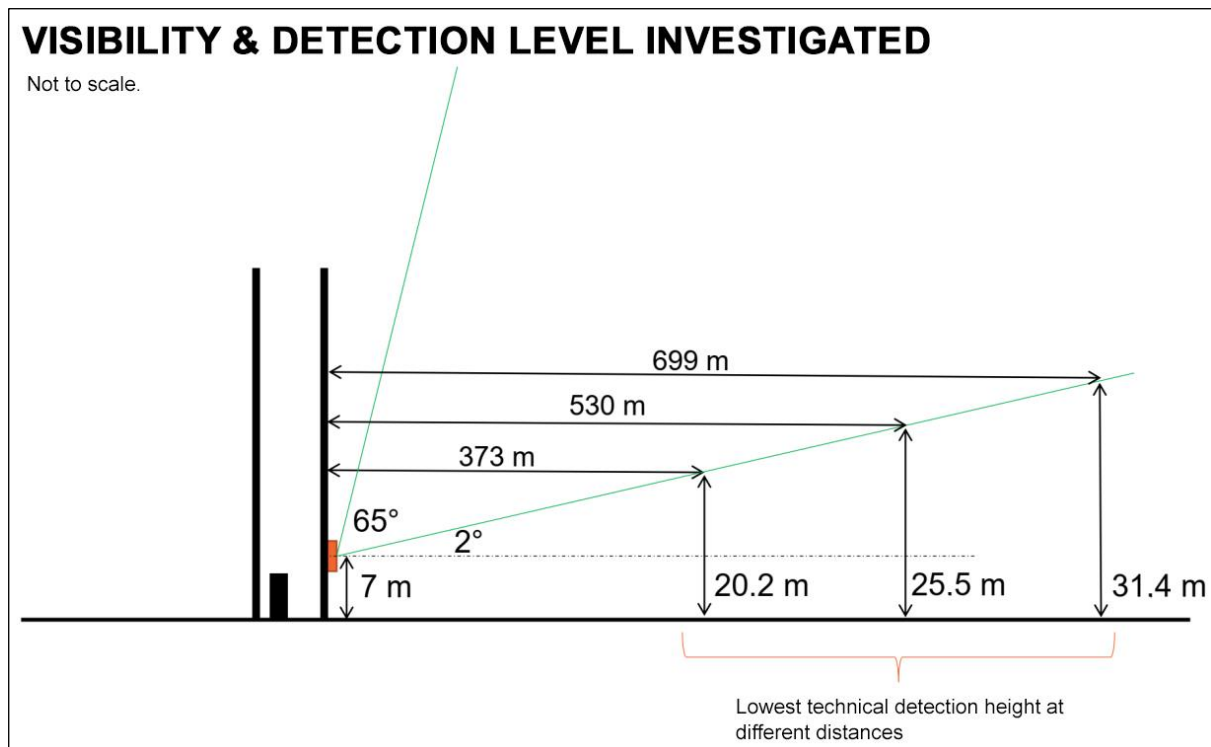
Fig. 3.1: Visibility and detection height of the Bioseco system at the Vestas V150 WT in Lentföhrden investigated by PNE.
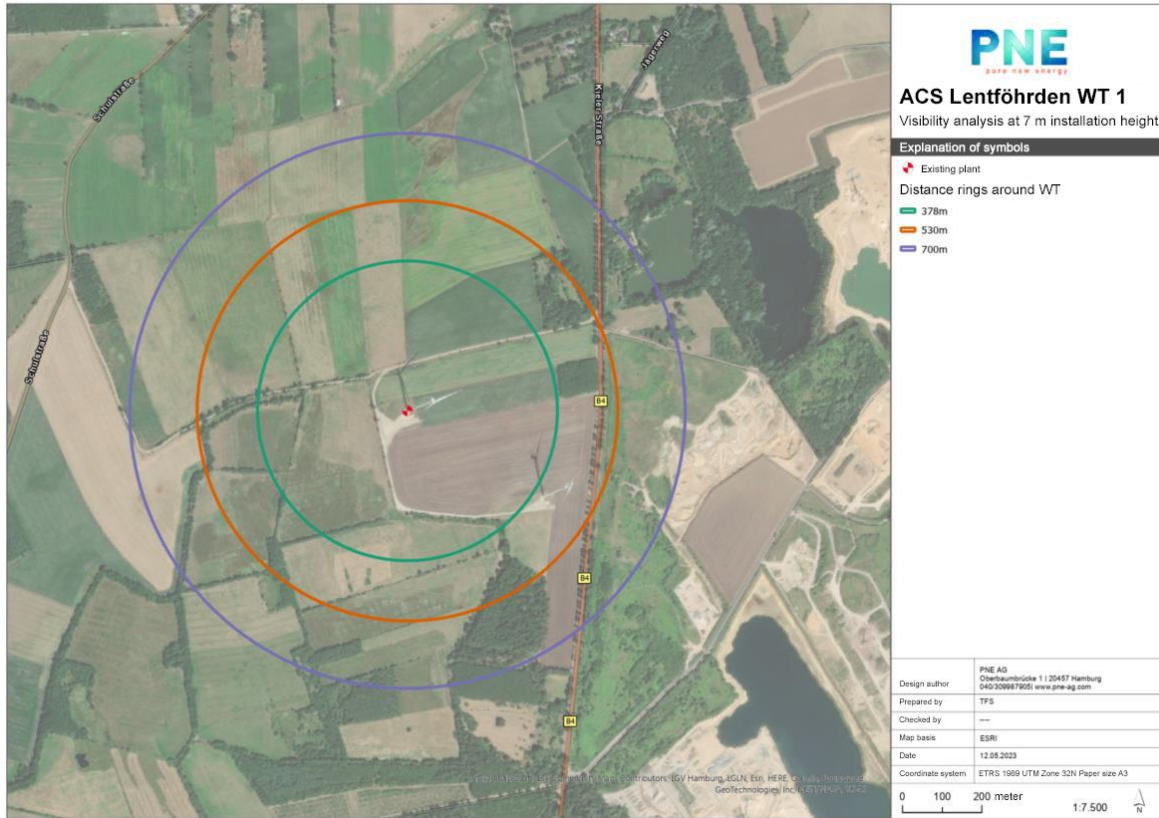
Fig. 3.2: Visibility analysis performed by PNE: Overall view of the three distances of 378 m, 530 m and 700 m (map unchanged, created by PNE on May 12, 2023).
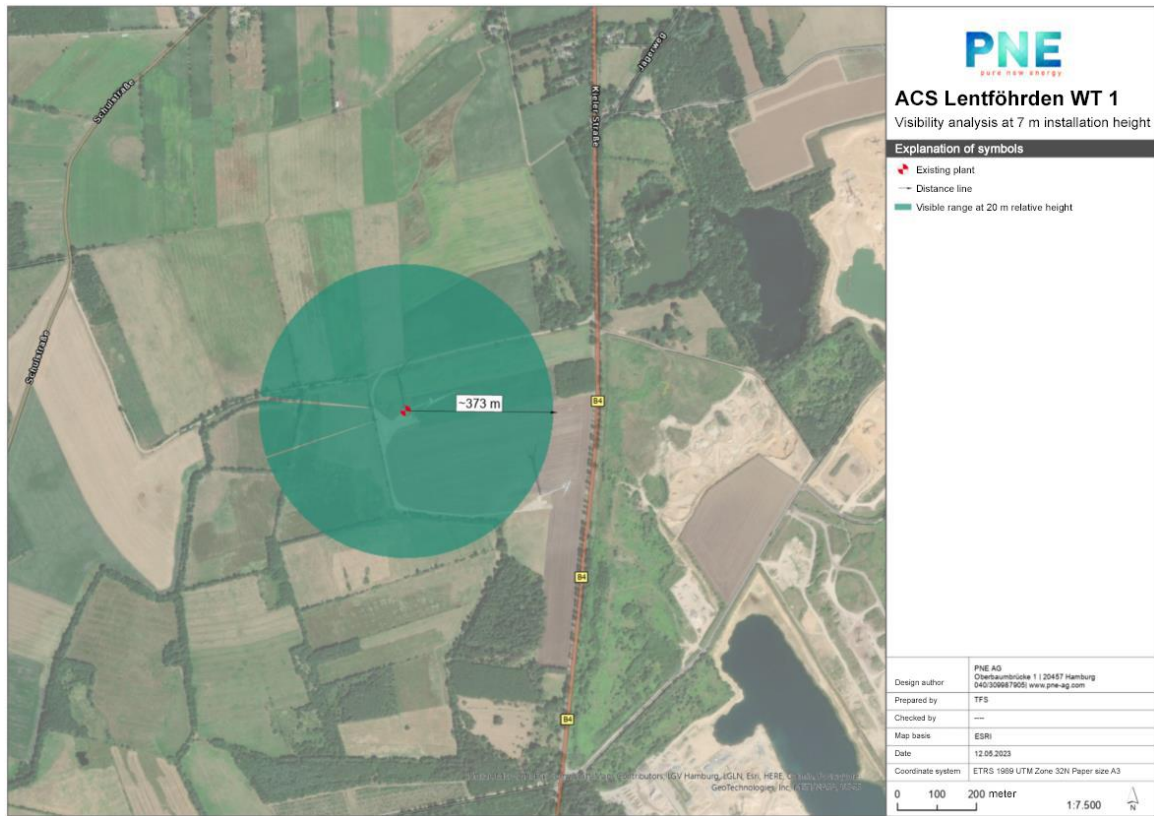
Fig. 3.3: Visibility analysis performed by PNE: Visible area at 20 m height (map unchanged, created by PNE on May 12, 2023).
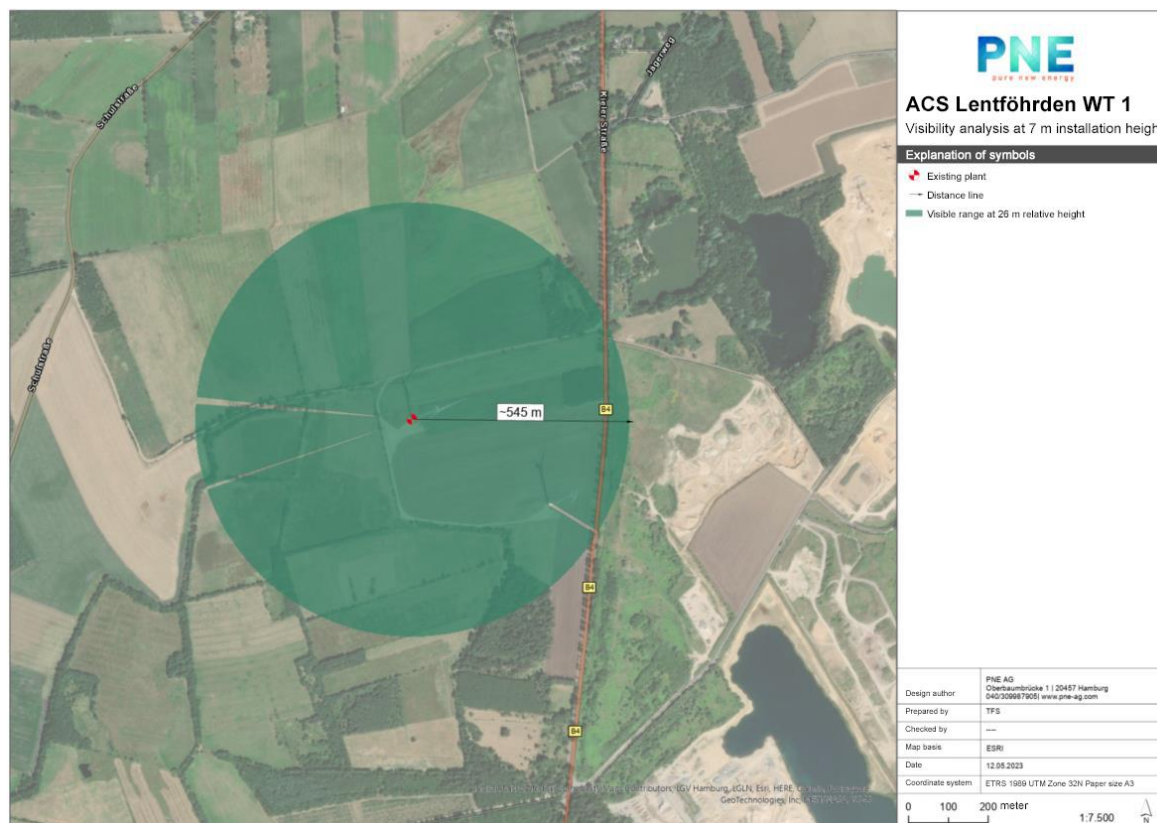
Fig. 3.4: Visibility analysis performed by PNE: Visible area at 26 m height (map unchanged, created by PNE on May 12, 2023).
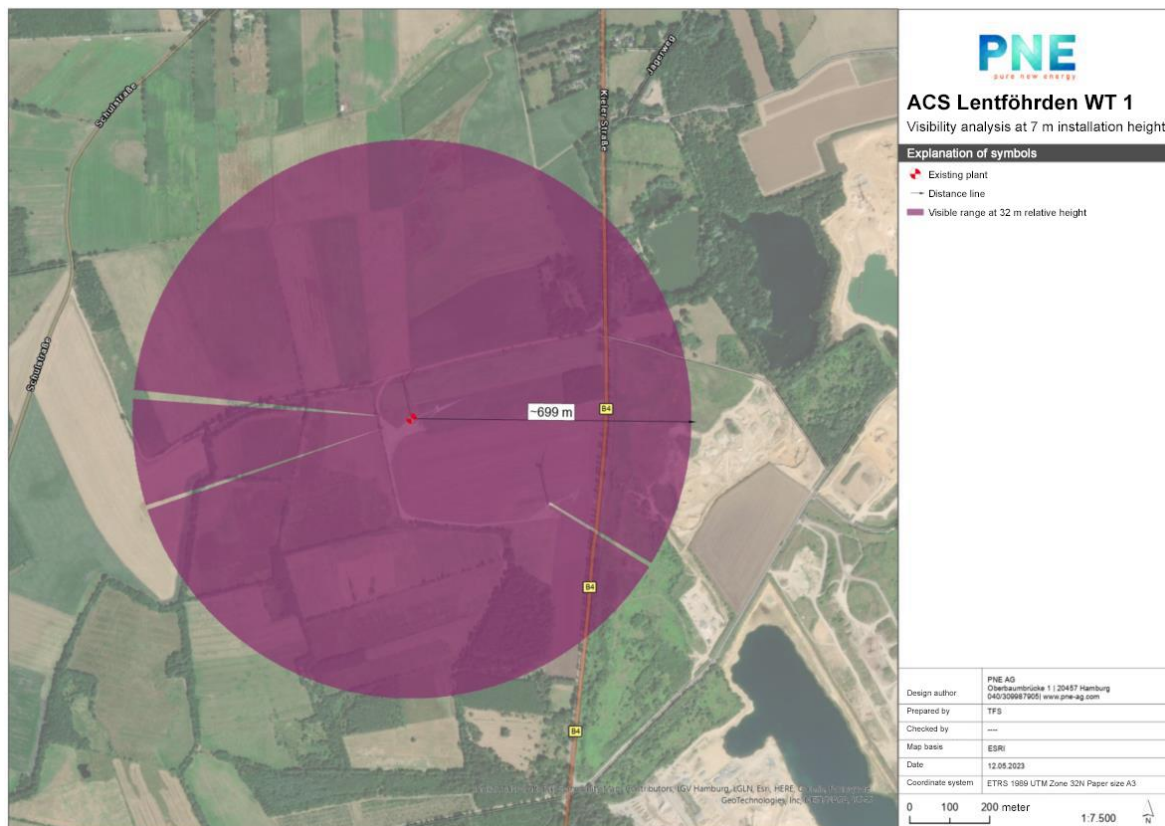
Fig. 3.5: Visibility analysis performed by PNE: Visible area at 32 m height (map unchanged, created by PNE on May 12, 2023).

The spatial coverage of the study site is not affected by any serious visual obscurations, so the Bioseco system has a very good initial situation in terms of topographic position and there are no elements that could affect the coverage rate (see section 1.1). The required coverage rates (see Table 3.1) of > 75% in the detection range and > 90% in the response range are met at the Lentföhrden site.

The visibility analysis (see Fig. 3.1) indicates that approaching low-flying birds with a flight altitude of ≤ 20.2 m are not detected by the system at a distance of 373 m, at a height of 25.5 m at a distance of 530 m, and at a flight altitude of 31.4 m at a distance of 699 m. In the present planning, the wind turbine has a lower rotor passage of 50 m and the approaching low-flying birds, which could possibly be overlooked or detected too late, are not in the danger zone of the rotating rotors. In reality, it is extremely unlikely that a low-flying bird will suddenly fly up into the rotor area.

3.2   Detection rates

With regard to the requirements for an ACS in terms of overall effectiveness, no "zero risk" is required (BVerwG judgment 9 A9.15 of April 28, 2016, item 141, 2016). The level of protection provided by the ACS must be sufficient to reduce the significantly increased risk of killing at each site for the corresponding target species below the significance threshold. Thus, some level of unprotected flight activity is permissible. A checklist provided by the KNE is intended, in the absence of statewide regulations, to assist agencies in assessing whether an ACS is a professionally recognized measure to reduce significantly increased risk of killing at a particular site for a particular target species (BRUNS et

al. 2021). Based on these minimum requirements, an assessment of the Bioseco system takes place (see Tab. 3.1).

According to the KNE (BRUNS et al. 2021), the detection range must cover at least the species-specific response distance of a target species. On top of this, there is the additional distance required for the recognition or classification time. The detection range must therefore be greater than the response distance. No fixed value is formulated by the KNE; the central requirement is that it at least corresponds to the species-specific response distance of the respective target species. A minimum value for the response range of 350 m, an orientation value of 500 m and an optimal value of 700 m were specified by the KNE as system-specific detection parameters (KNE GGMBH 2022). The more it exceeds the response distance, the higher the buffer for a timely response to put the WT into spin mode.

The calculated **species-specific response ranges** of **378 m** for the **red kite**, **511 m** for the **white stork**, and **529 m** for the white-tailed eagle (the latter two summarized as **530 m**, see section 2.4) are thus exactly within the detection ranges for the minimum requirements of the KNE.

The higher the detection rate, the higher the level of protection for the species in question. According to the KNE, a detection rate of 75% could constitute a lower limit. If the distance from the WT to the breeding site is shorter, or if very rare species at risk of collision are involved, higher detection rates of up to 90% may be required to achieve the required level of protection (see Table 3.1).

Tab. 3.1   Testing criteria from the KNE (according to BRUNS et al. 2021).

Testing criteria from the KNE	
Coverage rate at the site	
• Detection range	**> 75 %**
• Response range	**> 80 %**
• Main flight corridors	**> 90 %**
Detection range	
• Detection rate in the response range	**> 75 %**
Recognition rate	
• in the entire detection range	**> 75 %**
• in the response range	**> 90 %**

3.2.1   Detection rates in the respective response range:

The detection rate should clearly exceed 75% in the response range or at its outer boundary and ideally be at least 90% as an orientation value (BRUNS et al. 2021, see Tab. 3.1).

The results on the detection rate in the respective response range are shown for the red kite in Fig. 3.6, for the white-tailed eagle in Fig. 3.7 , and for the white stork in Fig. 3.8. All the three cases show, as expected, a decrease in the detection rate with increasing distance between LRF target and ACS. The detailed analyses can be found in the appendix (see Fig. A. .1 to Fig. A. .6).

The decisive factors are the detection rates in the respective response range of the species studied. Only if the wind power sensitive bird species or the target species is detected in time by the ACS, a

timely shutdown of the WT can take place or they can be put into spin mode and thus, the significantly increased killing risk of the respective species can be reduced.

All three bird species investigated – red kite, white-tailed eagle and white stork – were detected by the Bioseco system in the respective response range. The white-tailed eagle showed the clearest result with a 100% detection rate, followed by the white stork with 92.3% (simple) and 92.2% (GLMM). The red kite, with the smallest wingspan (1.4 m to 1.65 m) of the three species studied, showed the lowest value with 87.2% (simple) and 86.7% (GLMM). The results show that not only all mean detection rates were above the 75% required by the KNE (concerning the respective species-specific detection range – see above), but also the lower limits of the respective 95% confidence intervals – regardless of whether the simple or the GLMM-based method was used.

From a species protection perspective, all three target species are adequately recognized in the response range based on size classification. In order to reduce the significantly increased risk of killing, it is necessary to put the wind turbine into spin mode in good time when the target species ($\geq$ medium) approaches the response range of the wind turbine.

Red kite: $r_{Response}$= 378 m: detection rate simple: **87.2%**, detection rate GLMM: **86.7%**

White stork: $r_{Response}$= 530 m: detection rate simple: **92.3%**, detection rate GLMM: **92.2%**

White-tailed eagle: $r_{Response}$= 530 m: detection rate simple: **100%**, detection rate GLMM: **100%**

Fig. 3.6: Statistical results of the red kite detection rate. GLMM analyses (left) vs. the "simple" approach (right) based on a detection radius of 378 m (≤ the response radius – see above). Red dots indicate mean values, black bars 95% confidence intervals. N_LRF indicates the number of underlying LRF points.
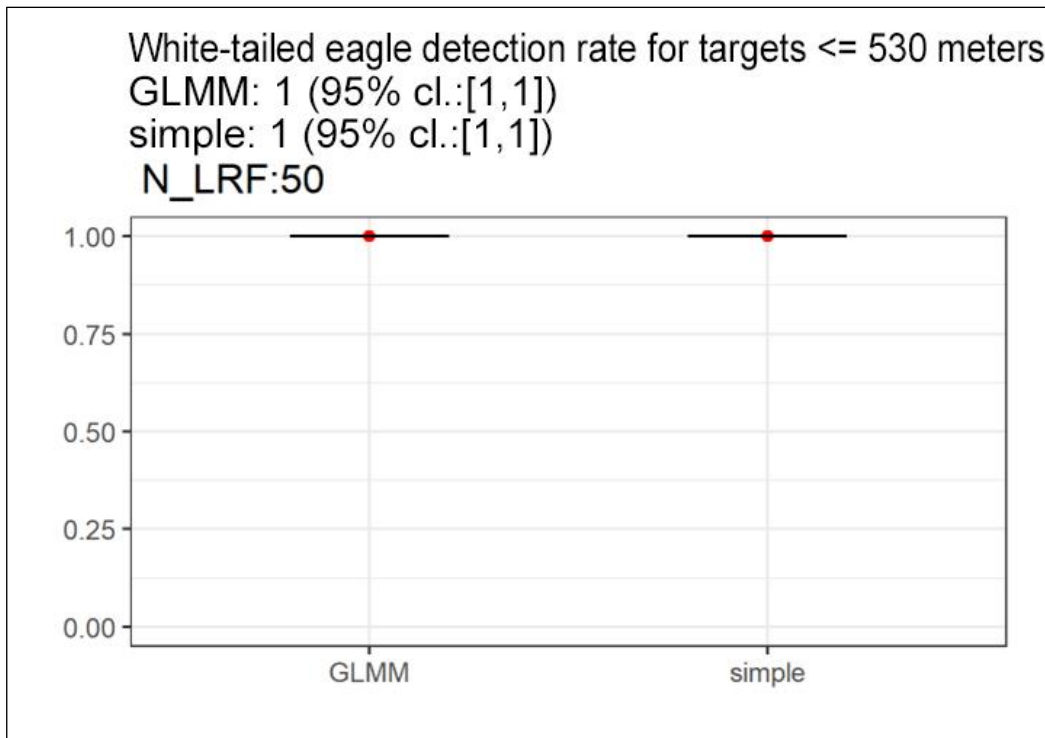
Fig. 3.7: Statistical results of the white-tailed eagle detection rate. GLMM analyses (left) vs. the "simple" approach (right) based on a detection radius of 530 m (≤ the response radius – see above). Red dots indicate

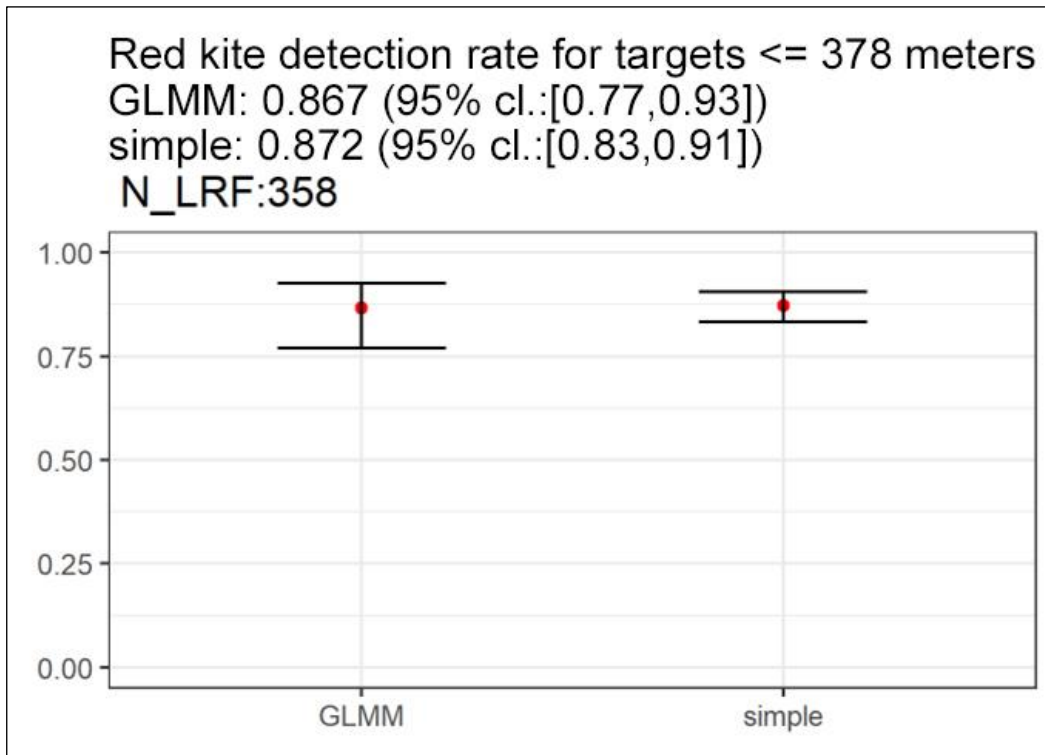mean values, black bars 95% confidence intervals. N_LRF indicates the number of underlying LRF points.

Fig. 3.8: Statistical results of the white stork detection rate. GLMM analyses (left) vs. the "simple" approach (right) based on a detection radius of 530 m (≤ the response radius – see above). Red dots indicate mean values, black bars 95% confidence intervals. N_LRF indicates the number of underlying LRF points.
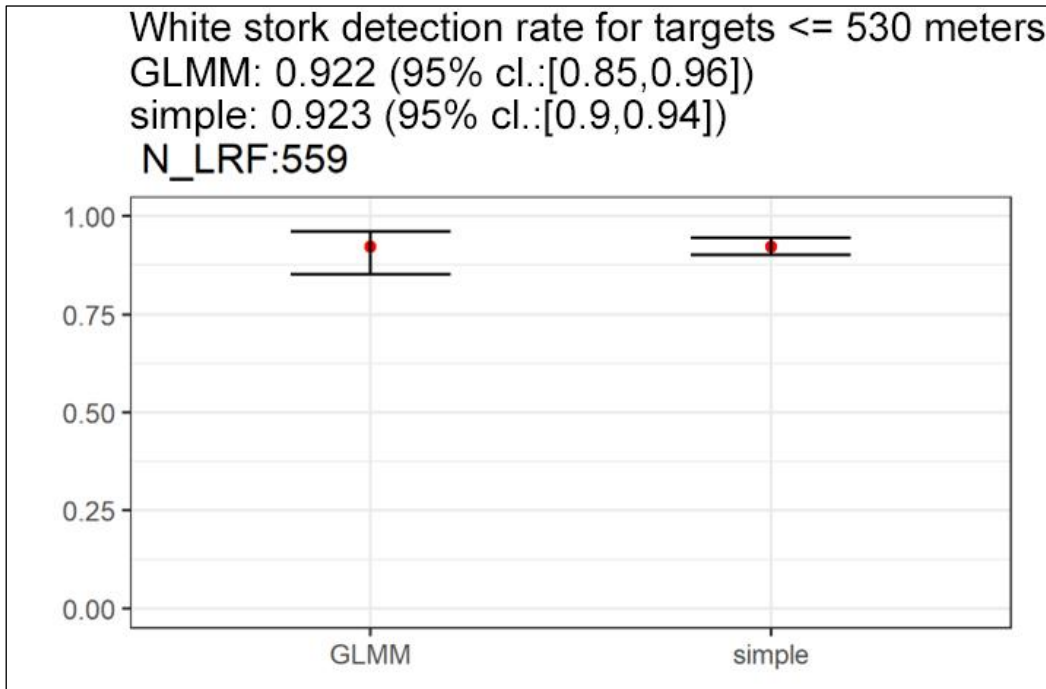
The detection rate goes far beyond the response range and thus complies with the KNE criteria (see Appendix A.3).

3.3 Size classification

For classification analysis, data from the LRF with species identification, e.g. red kite, will be matched and analyzed with data from the ACS ≥ medium.

The recognition rate results are shown for the red kite in Fig. 3.9 , for the white-tailed eagle in Fig. 3.10 and for the white stork in Fig. 3.11.Detailed analyses can be found in the appendix (Fig. A. .1 to Fig. A. .6). In all cases, there was little or no decrease in recognition rate with increasing distance between LRF target and ACS, as overall recognition rates were very high. According to the KNE checklist, the detection rate in the reaction area or at its outer edge should be well above 75% and ideally 90%. The Bioseco system recognizes the three species > medium well above the required 75%, regardless of the selected method: simple or GLMM. However, results of 90% are not reached. According to the KNE, the reduction of the significantly increased risk of death is not automatically fulfilled when the lower limit of 75% is reached. In individual cases, higher detection rates may be required and then considered on a project-specific basis.

Recognition rates in the respective response range:

Red kite: $r_{reaction}$= 378 m: simple detection rate: **84.6%**, GLMM detection rate: **90.0%**

White stork: $r_{reaction}$= 530 m: simple detection rate: **86.8%,** GLMM detection rate: **87.4%**

White-tailed eagle: $r_{reaction}$= 530 m: simple detection rate: **87.4%**, GLMM detection rate: **87.4%**

Red kite recognition rate (>=medium) for targets <= 378 meters
GLMM: 0.983 (95% cl.:[0.94,1])
simple: 0.929 (95% cl.:[0.9,0.96])
 N_LRF:312

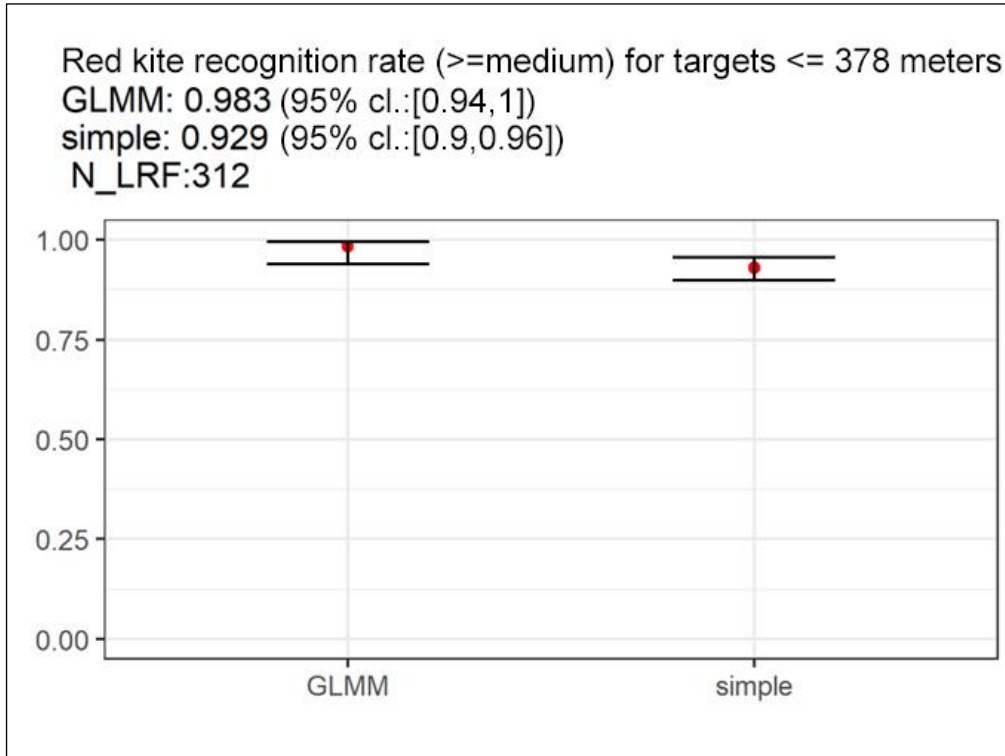*Fig. 3.9: Statistical results of the red kite recognition rate. GLMM analyses (left) vs. the "simple" approach (right) based on a detection radius of 378 m (≥ the response radius – see above). Red dots indicate mean values, black bars 95% confidence intervals. . The latter do not include the uncertainties of the correction step (see main text).N_LRF indicates the number of underlying LRF points.*
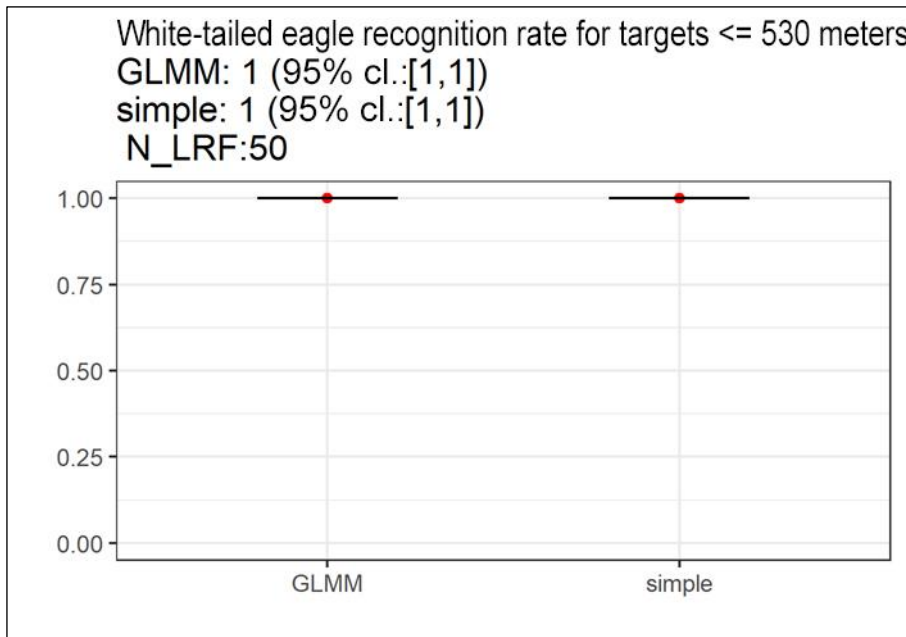
Fig. 3.10: Statistical results of the white-tailed eagle recognition rate. GLMM analyses (left) vs. the "simple" approach (right) based on a detection radius of 530 m (≥ the response radius – see above). Red dots indicate mean values, black bars 95% confidence intervals. . The latter do not include the uncertainties of the correction step (see main text). N_LRF indicates the number of underlying LRF points.

Fig. 3.11: Statistical results of the white stork recognition rate. GLMM analyses (left) vs. the "simple" approach (right) based on a detection radius of 530 m (≥ the response radius – see above). Red dots indicate mean values, black bars 95% confidence intervals. The latter do not include the uncertainties of the correction step (see main text). N_LRF indicates the number of underlying LRF points.
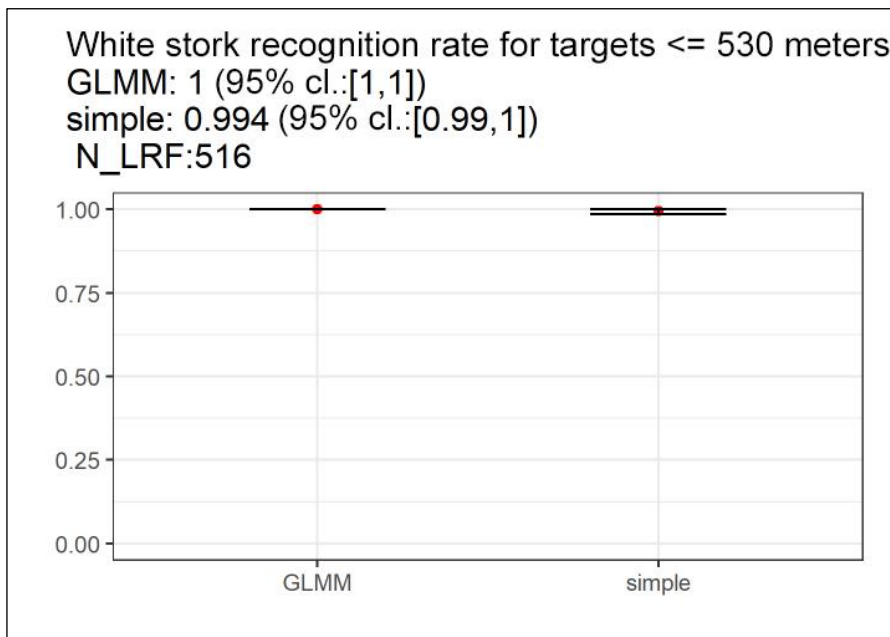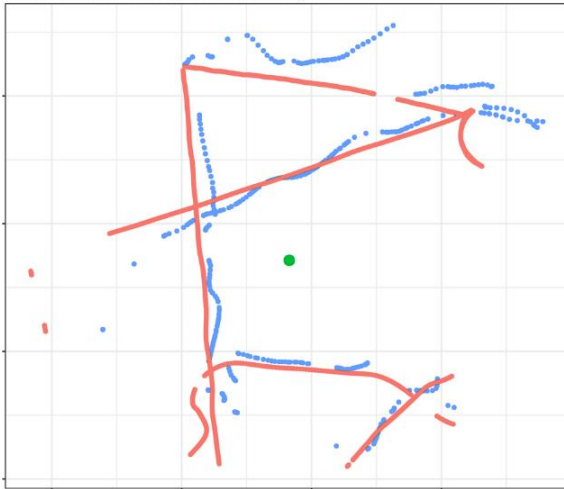
3.4 The three species examined (> medium or red kite, white stork and white-tailed eagle) were detected with a detection rate of > 75% and thus meet the lower limit of the required criterion of the KNE checklist. Thus, in terms of species protection, all three species are detected and sufficiently recognized as > medium and the WT can be put into spin mode to reduce the significantly increased risk of death for each species. A higher detection rate may be required in individual projects, which would then have to be tested and verified on a project-specific basis.Position accuracy

The final number of data points used were N=2,317, N= 1,295 and N=1,599. The mean and median values of the relative local error (i.e., the amount of distance divided by the distance between the target and the WT) can be found for the three different flights given in Fig. 3.12. It turns out that the mean is about 0.1, ergo f_{RDE} = 1.1. Further analyses showed that the relative local error does not or only insignificantly increases with distance, i.e. it can also be assumed to be 0.1 at the edge of the response range (see Fig. 2.8 center/bottom).

Fig. 3.12: Center/top: GPS points from three different drone flights (red dots) vs. assigned ACS points (blue dots) in the 500-meter vicinity of the WT (green dot). Center/bottom: The relative local error (mean) for the three different flights as a function of the distance between WT and target. Shaded areas: 95% confidence intervals.

35

The respective response ranges of the target species are up to 530 m, an RDE of approx. 10% was determined in this range (drone flight 1 = 13%, drone flight 2 = 9%, and drone flight 3 = 11%).

3.5 False shutdown rate

The false shutdown rate has a very strong influence on the economic efficiency and not on the species protection requirements and is therefore not part of this report.

4   CONCLUSIONS

4.1   Summary assessment and comments

The statistical analyses of the empirical data show that for all three target species (red kite, white-tailed eagle and white stork), the requirements from the KNE Checklist are met. The following species-specific response radii were calculated for each target species:

Red kite: r_{Response}= 377.98 m

White stork: r_{Response}= 511.93 m

White-tailed eagle: r_{Response}= 528.99 m,

based on an empirically determined relative local error of about 10%, averages to species-specific flight speeds available in the literature, and empirically determined times of signal propagation and of putting into spin mode.

Detection and recognition rates were determined using two different statistical techniques ("simple" vs. "GLMM"). The detection rates for the above response ranges are well above the required 75% in all three cases:

Red kite: r_{Response}= 378 m: detection rate simple: 87.2%, detection rate GLMM: 86.7%

White stork: r_{Response}= 530 m: detection rate simple: 92.3%, detection rate GLMM: 92.2%

White-tailed eagle: r_{Response}= 530 m: detection rate simple: 100%, detection rate GLMM: 100%,

and the recognition rates are also above the required lower limit of 75% in all three cases:

Red kite: r_{Response}= 378 m: recognition rate simple: 84,6%, recognition rate GLMM: 90%

White stork: r_{Response}= 530 m: recognition rate simple: 86,8%, recognition rate GLMM: 87,4%

White-tailed eagle: r_{Response}= 530 m: recognition rate simple: 87,4%, recognition rate GLMM: 87,4%.

For an even more differentiated view, the continuous change of the above rates as a function of the distance between target and ACS was also shown. It should also be noted that all confidence intervals determined for the rates include values not smaller than the above-mentioned 75% and 90%; the estimates are therefore associated with a high degree of certainty.

Data manipulation was excluded by first sending the ACS data from Bioseco to BioConsult SH and then providing the LRF data by BioConsult SH.

In summary, it can be concluded that the Bioseco system adequately detects the target species red kite, white stork and white-tailed eagle with respect to KNE requirements and classifies them based on size.

In this context, however, it should be noted that the above response radii were determined in many respects from a precautionary point of view. The conservative assumptions in this regard are:

- The worst-case scenario is assumed that the bird's direction of flight, as seen from the edge of the response range, is not tangential but points directly at the rotor area;

- Using the real flight speeds in the above formula implies that the bird is flying in a straight line. This is usually not the case; e.g., when foraging and/or taking advantage of thermals, birds usually fly in a highly non-linear manner, so that the effective approach speed may be significantly lower;

- Adding the rotor blade length to the response range (see formula) implies that the bird flies in alignment with the rotor blade disc, i.e., the tips of the rotor blades point toward the bird. This is a very unrealistic scenario;

- Multiplying the relative local error in the above formula assumes that the misestimation of the bird's position by the ACS is in favor of increased bird strike risk. However, it must rather be assumed that the error has an effect half in favor and half to the disadvantage of an increased risk.

In addition, it should be noted that the response radii calculated above are also unnecessarily increased by the ACS-independent fact that signal prioritization in the context of wind farm control results in a relatively high value of $t_{Latency}$.

Bioseco indicates protection for target species ≥ medium through event-related shutdowns of wind turbines.

The fulfillment of the species protection requirements are met in terms of the required minimum requirements from the KNE for the Bioseco system.

5   LITERATURE

ASCHWANDEN, J., WANNER, S. & LIECHTI, F. (2015): Investigation on the effectivity of bat and bird detection at a wind turbine: Final Report Bird Detection. Swiss Ornithological Institute/Sempach (SUI), p. 34.

BIONUM GMBH (2023): Statistical evaluation of the "Bioseco" anti-collision system in the context of the "KNE Checklist" Dipl.-Math. Dipl.-Biol. Dr. Moritz Mercker Bionum GmbH – Biostatistics Office Finkenwerder Norderdeich 15A 21129 Hamburg.

BOLKER, B. M., BROOKS, M. E., CLARK, C. J., GEANGE, S. W., POULSEN, J. R., STEVENS, M. H. H. & WHITE, J.-S. S. (2009): Generalized linear mixed models: a practical guide for ecology and evolution. *Trends in Ecology and Evolution* 24/3, pp. 127–135.

BRUDERER, B. & BOLDT, A. (2001): Flight characteristics of birds: I. radar measurements of speeds. *Ibis* 143/2, Citation Key: brudererFlightCharacteristicsBirds2001, pp. 178–204.

BRUNS, E., ASCHWANDEN, J., MUSIOL, F., FRÜH, D., KLEYHEEG-HARTMAN, J., SPRÖTGE, M., REICHENBACH, M., REERS, H., MEHRGOTT, H., WEISS, A., & SCHUSTER, E. - **BRUNS, E. ET AL** (2019): KNE conference on bird protection at wind turbines – detection systems as an opportunity for nature-friendly wind energy development? Documentation of the KNE conference of May 15 and 16, 2019 in Kassel (Kompetenzzentrum Naturschutz und Energiewende KNE gGmbH, ed.; p. 58). X:\04_Literatur\01_Literatur_(NICHT_BEARBEITEN!)\KNE_2019_Dokumenta-tion_vogelschutz_an_windenergieanlagen_detektionssysteme_als_chance_fuer_ei-nen_naturvertraeglichen_windenergieausbau.pdf.

BRUNS, E., SCHUSTER, E. & STREIFFELER, J. (2021): Requirements for technical monitoring and shutdown systems at wind turbines, BfN-Skripten. No. 610, Federal Agency for Nature Conservation/Bonn – Bad Godesberg (DEU).

CANTY, A. J., DAVIDSON, A. C., HINKLEY, D. V., & VENTURA, V. (2006): Bootstrap diagnostics and rem-edies. The Canadian Journal of Statistics, 34(1), 5–27. https://doi.org/Added.

CARPENTER, J., & BITHELL, J. (2000): Bootstrap confidence intervals: When, which, what? A practical guide for medical statisticians. Statistics in Medicine, 19(9), 1141–1164. https://doi.org/Added.

FIELD, A., MILES, J., & FIELD, Z. (2012): Discovering statistics using R. SAGE Publications Ltd. https://doi.org/Added.

FRÜH, D. & STARK, H. (2020): Endbericht Raumnutzungsanalyse Großvögel im Windpark Osterburg. *Sachsen-Anhalt, Landkreis Stendal.*

GPS STANDARD POSITIONING SERVICE – **GPS ACCURACY** (n.d.). https://www.gps.gov/technical/ps/2007- PPS-performance-standard.pdf.

HASTIE, T., & TIBSHIRANI, R. J. (1990): Generalized Additive Models. London, UK: Chapman and Hall. https://doi.org/Added.

HURLBERT, S. H. (1984): Pseudoreplication and the Design of Ecological Field Experiments. Ecological Monographs, 54(2), 187–211. https://doi.org/Added.

JANNES KREUTZFELDT, PNE - **J. KREUTZFELD** (2023): Visibility analysis Bioseco Longe Range BPS procedure and calculation.

JENSEN, F. P., RINGGAARD, R., BLEW, J. & JACOBSEN, E. M. (2016): Anholt Offshore Wind Farm. Post-construction monitoring of bird migration. Report on raptor migration survey in 2014–2016., Final Report. Roskilde (DNK), p. 83.

KNE GGMBH (2022): BWE specialist conference on wind energy and species protection: Advancing the energy turnaround – climate and species protection considered together – May 31, 2022 Hanover. Requirements for anti-collision systems for birds – areas of application, avoidance effectiveness, need for clarification.

KORNER-NIEVERGELT, F., ROTH, T., VON FELTEN, S., GUELAT, J., ALMASI, B., & KORNER-NIEVERGELT, P. (2015): Bayesian Data Analysis in Ecology Using Linear Models with R, BUGS, and Stan. Elsevier, London. https://doi.org/Added.

MERCKER, M., LIEDKE, J., LIESENJOHANN, T. & BLEW, J. (2023): Pilot study "Testing of probabilistic methods": Testing of probabilistic methods with regard to their technical prerequisites with the aim of validating the method for determining the project-related killing risk of breeding bird species at risk of collision at wind energy plants. *Pilot study on behalf of the Hessian Ministry for the Environment, Climate Protection, Agriculture and Consumer Protection (HMUKLV)*.

Pennycuick, C. J. (2001): Speeds and wingbeat frequencies of migrating birds compared with calculated benchmarks. *Journal of Experimental Biology* 204/19, pp. 3283–3294.

PENNYCUICK, C. J., ÄKESSON, S. & HEDENSTRÖM, A. (2013): Air speeds of migrating birds observed by ornithodolite and compared with predictions from flight theory. *Journal of The Royal Society Interface* 10/86.

PINHEIRO, J. C., & BATES, D. M. (2000): Mixed-effect models in S and S-Plus. New York: Springer Verlag. https://doi.org/Added.

PNE (2023): Bioseco Anti-Collision System Pilot Study – Interim Report & Transferability. PNE Dept. of Technologies: Janne Brandt, Lukas Krohn, Jannes Kreutzfeld and Carsten Bührer.

RANSOM, D.,, & PINCHAK, W. E. (2003): Ransom, D., & Pinchak, W. E. (2003). Assessing Accuracy of a Laser Rangefinder in Estimating Grassland Bird Density. Wildlife Society Bulletin (19732006), 31(2), 460–463.

SKOV, H., DESHOLM, M., HEINÄNEN, S., JOHANSEN, T. W. & THERKILDSEN, O. R. (2015): Kriegers Flak Offshore Wind Farm. Birds and Bats. EIA -Technical report. Aarhus University, DCE – Danish Centre for Environment and Energy & DHI Group, p. 196.

SKOV, H., HEINÄNEN, S., NORMAN, T., WARD, R., MENDEZ-ROLDAN, S. & ELLIS, I. (2018): ORJIP Bird Collision and Avoidance Study, Final Report. The Carbon Trust/London (GBR), p. 247.

SPAAR, R. (1997): Flight strategies of migrating raptors; a comparative study of interspecific variation in flight characteristics. *Ibis* 139/3, pp. 523–535. DoI: 10.1111/j.1474-919X.1997.tb04669.x, ISSN: 1474-919X.

TENNEKES, H. (1997): Appendix: Data of selected birds. In: *Hummingbirds and Jumbo Jets: The Simple Art of Flying* Birkhäuser Verlag, pp. 157–176.

WOOD, S. R. (Hrsg.) (2017): Generalized additive models. An intoduction with R. CRC Press/Boca Raton (USA).

ZUUR, A. F. (2012): A beginner's guide to generalized additive models with R. Highland Statistics Ltd. https://doi.org/Added.

ZUUR, A., IENO, E., & SMITH, G. M. (2007): Analysing Ecological Data. Springer Science+Business Media, LLC. https://doi.org/Added.

ZUUR, A. F., IENO, E. N., WALKER, N. J., SAVELIEV, A. A. & SMITH, G. M. (2009): Mixed effects models and extensions in ecology with R. Reihe: Statistics for Biology and Health, Springer/New York, NY (USA), 574 p.

(2016): BVerwG, judgment of April 28, 2016 – 9 A9.15.

A   APPENDIX

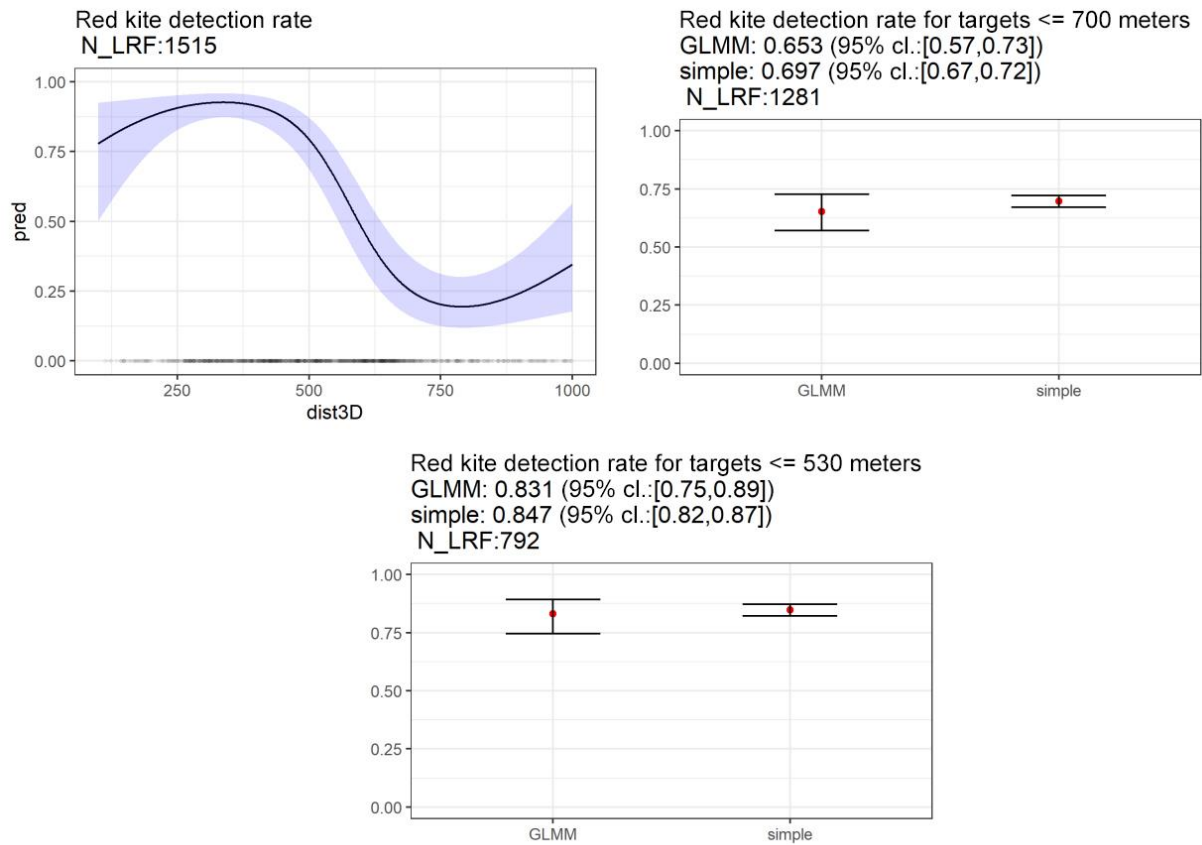## A.1 Detection rate

A.1.1   Red kite

Fig. A.1   Statistical results of the red kite detection rate. Top left: Detection rate as a (possibly nonlinear) function of the distance between LRF point and ACS based on GAMM analyses. Black line: Detection rate, purple area: 95% confidence intervals. Semi-transparent points just above the X-axis indicate the existence of individual measurement points. Remaining figures: GLMM analyses (in each case, on the left) vs. the "simple" approach (in each case, on the right) based on different detection radii (see respective caption). Red dots indicate mean values, black bars 95% confidence intervals. N_LRF indicates the number of underlying LRF points
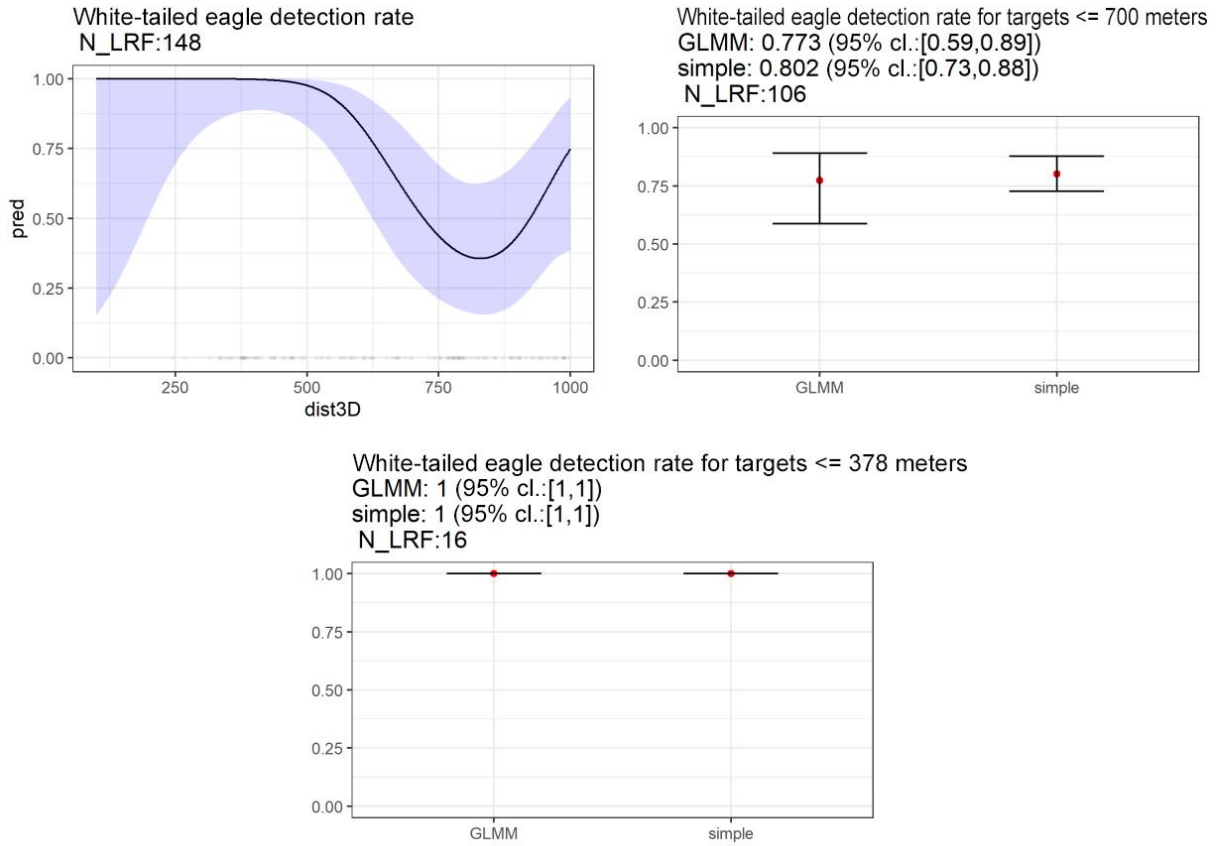
A.1.2   White-tailed eagle

Fig. A.A.2   *Statistical results of the white-tailed eagle detection rate. Top left: Detection rate as a (possibly nonlinear) function of the distance between an LRF point and ACS based on GAMM analyses. Black line: detection rate, purple-shaded area: 95% confidence intervals. Semi-transparent points just above the X-axis indicate the existence of individual measurement points. Remaining figures: GLMM analyses (in each case, on the left) vs. the "simple" approach (in each case, on the right) based on different detection radii (see respective caption). Red dots indicate mean values, black bars 95% confidence intervals. N_LRF indicates the number of underlying LRF points.*
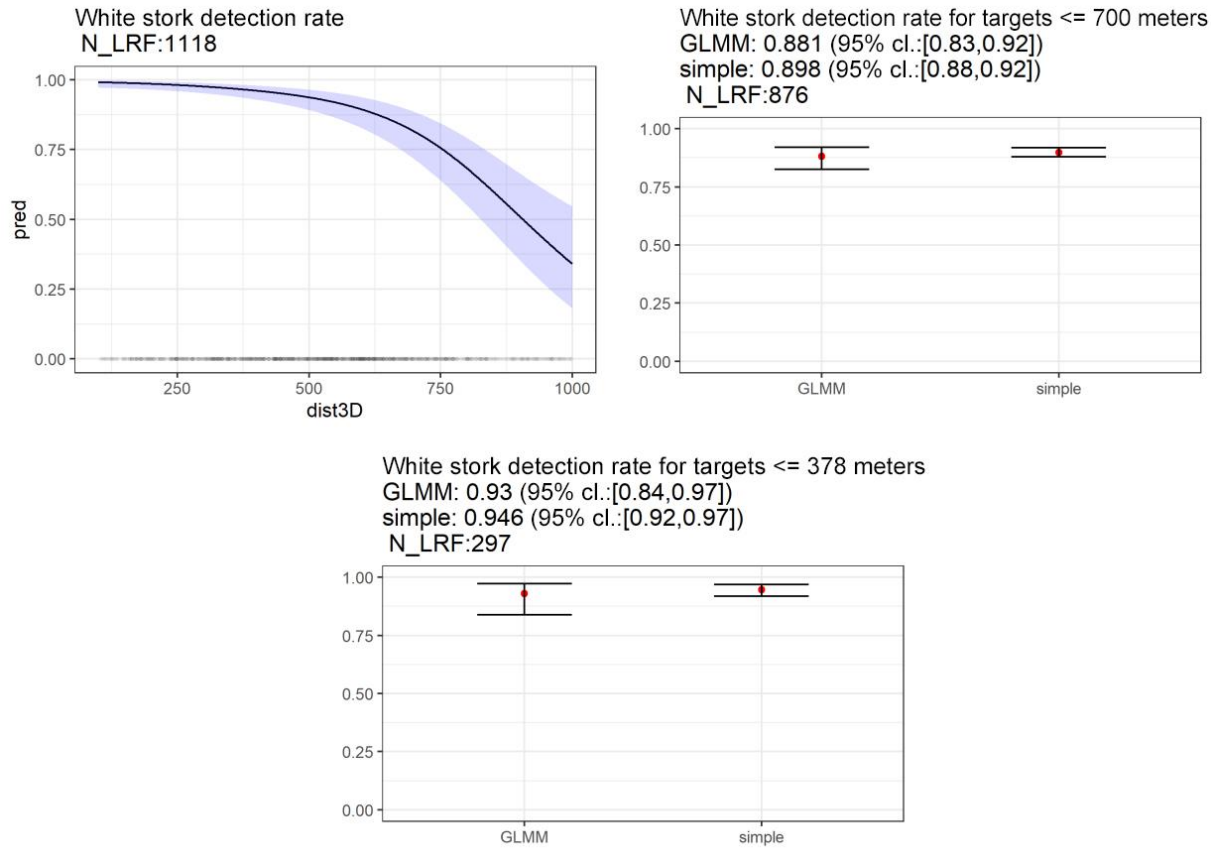
A.1.3 White stork

Fig. A.A.3   *Statistical results of the white stork detection rate. Top left: Detection rate as a (possibly nonlinear) function of the distance between an LRF point and ACS based on GAMM analyses. Black line: Detection rate, purple area: 95% confidence intervals. Semi-transparent points just above the X-axis indicate the existence of individual measurement points. Remaining figures: GLMM analyses (in each case, on the left) vs. the "simple" approach (in each case, on the right) based on different detection radii (see respective caption). Red dots indicate mean values, black bars 95% confidence intervals. N_LRF indicates the number of underlying LRF points.A.2 Recognition rate*

A.2 Recognition rate
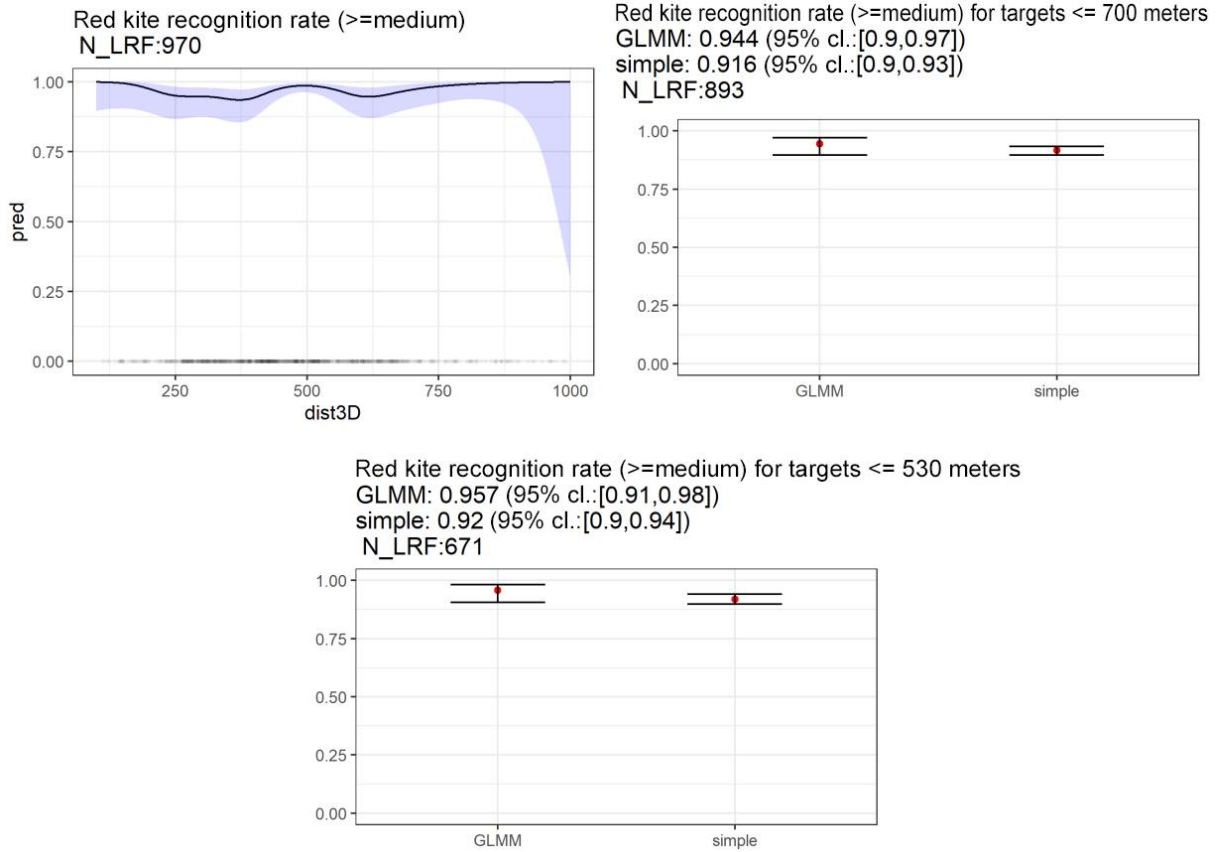
A.2.1 Red kite

Fig. A.A.4   *Statistical results of the red kite detection rate. Top left: Detection rate as a (possibly nonlinear) function of the distance between an LRF point and ACS based on GAMM analyses. Black line: uncorrected detection rate, red line: corrected detection rate, purple shaded area: 95% confidence intervals for the uncorrected rate. Semi-transparent points just above the X-axis indicate the existence of individual measurement points. Remaining figures: GLMM analyses (in each case, on the left) vs. the "simple" approach (in each case, on the right) based on different detection radii (see respective caption). Red dots indicate mean values, black bars 95% confidence intervals. The latter do not include the uncertainties of the correction step (see main text). N_LRF indicates the number of underlying LRF points.*
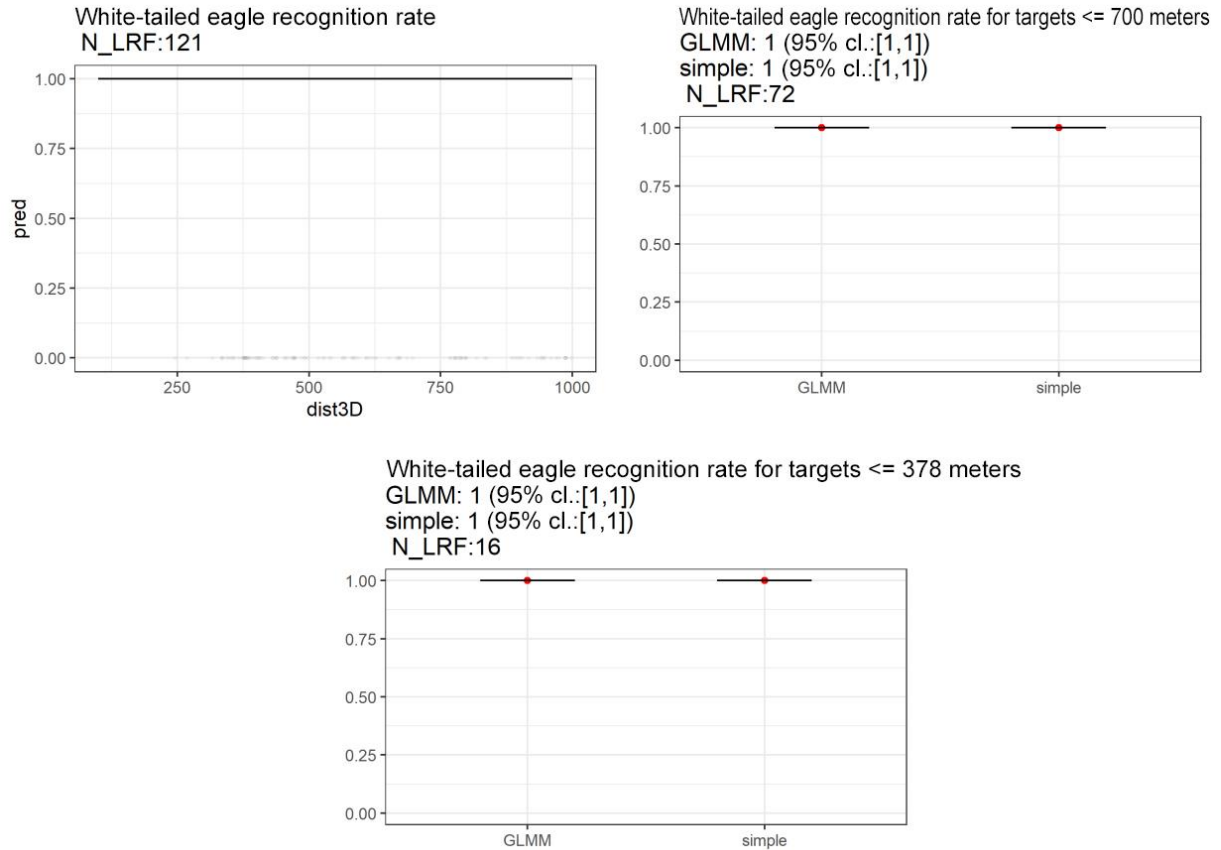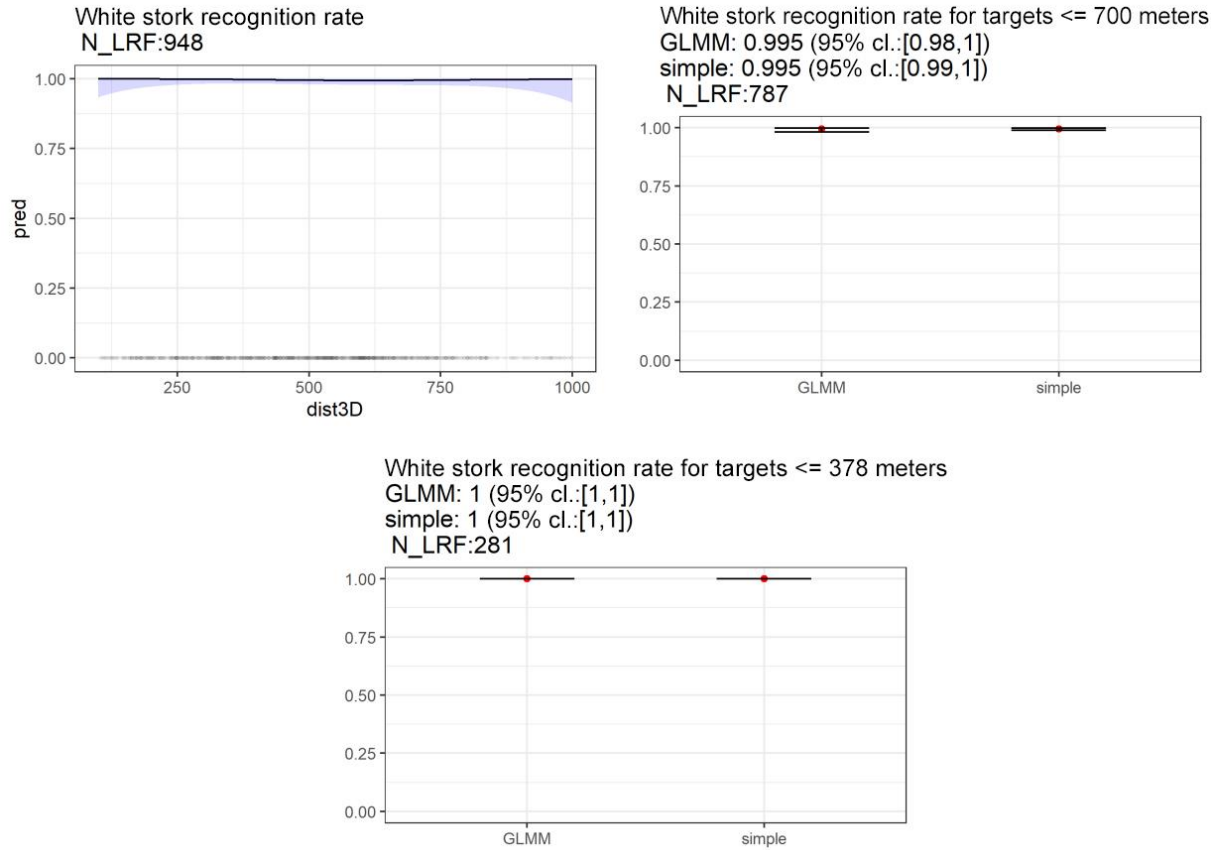
A.2.2 White-tailed eagle

Fig. A.A.5   *Statistical results of the white-tailed eagle detection rate. Top left: Detection rate as a (possibly nonlinear) function of the distance between an LRF point and ACS based on GAMM analyses. Black line: uncorrected detection rate, red line: corrected detection rate, purple shaded area: 95% confidence intervals for the uncorrected rate.Semi-transparent points just above the X-axis indicate the existence of individual measurement points. Remaining figures: GLMM analyses (in each case, on the left) vs. the "simple" approach (in each case, on the right) based on different detection radii (see respective caption). Red dots indicate mean values, black bars 95% confidence intervals. The latter do not include the uncertainties of the correction step (see main text).N_LRF indicates the number of underlying LRF points.*

A.2.3 White stork

White stork recognition rate
N_LRF:948

White stork recognition rate for targets <= 700 meters
GLMM: 0.995 (95% cl.:[0.98,1])
simple: 0.995 (95% cl.:[0.99,1])
N_LRF:787

White stork recognition rate for targets <= 378 meters
GLMM: 1 (95% cl.:[1,1])
simple: 1 (95% cl.:[1,1])
N_LRF:281

A.3 Detection rates outside the respective response range (700 m)

The results on the detection rate outside the respective response range ≤ 700 m indicated a decrease in the rate, as expected. Again, the values showed a similar result for each species, regardless of the choice of method whether simple or GLMM-based. However, white storks showed here the highest detection rate with 89.8% (simple, GLMM 88.1%, see Fig. A.9), followed by the white-tailed eagle with 77.3% (simple, GLMM 80.2%, see Fig. A.8). The smallest of the three species surveyed, the red kite, again showed the lowest detection rate at 69.7% (simple, GLMM 65.3%, see Fig. A.7). The detection values outside the response range showed, despite the greater distance, high values of at least approx. 70%.

Red kite: $r_{Response}$= ≤ 700 m: detection rate simple: **69.7%**, detection rate GLMM: **65.3%**

White stork: $r_{Response}$= ≤ 700 m: detection rate simple: **89.8%**, detection rate GLMM: **88.1%**

White-tailed eagle: $r_{Response}$= ≤ 700 m: detection rate simple: **77.3%**, detection rate GLMM: **80.2%**

Fig. A.6: Statistical results of the red kite detection rate. GLMM analyses (left) vs. the "simple" approach (right) based on a detection radius of 700 m (≥ the response radius up to max. 700 m). Red dots indicate mean values, black bars 95% confidence intervals. N_LRF indicates the number of underlying LRF points.
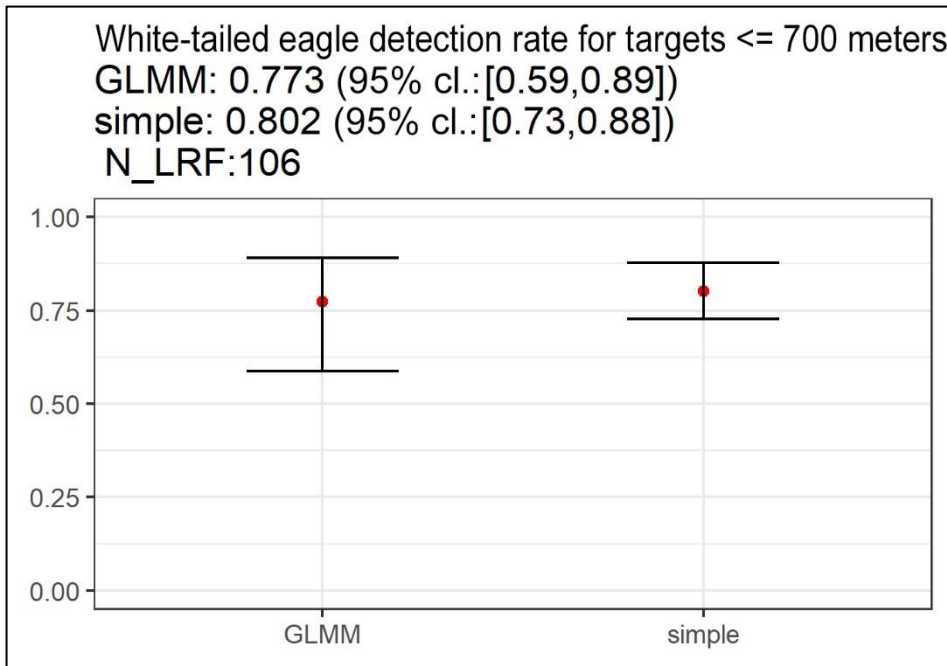
Fig. A.7: Statistical results of the white-tailed eagle detection rate. GLMM analyses (left) vs. the "simple" approach (right) based on a detection radius of 700 m (≥ the response radius up to max. 700 m). Red dots indicate mean values, black bars 95% confidence intervals. N_LRF indicates the number of underlying LRF points.
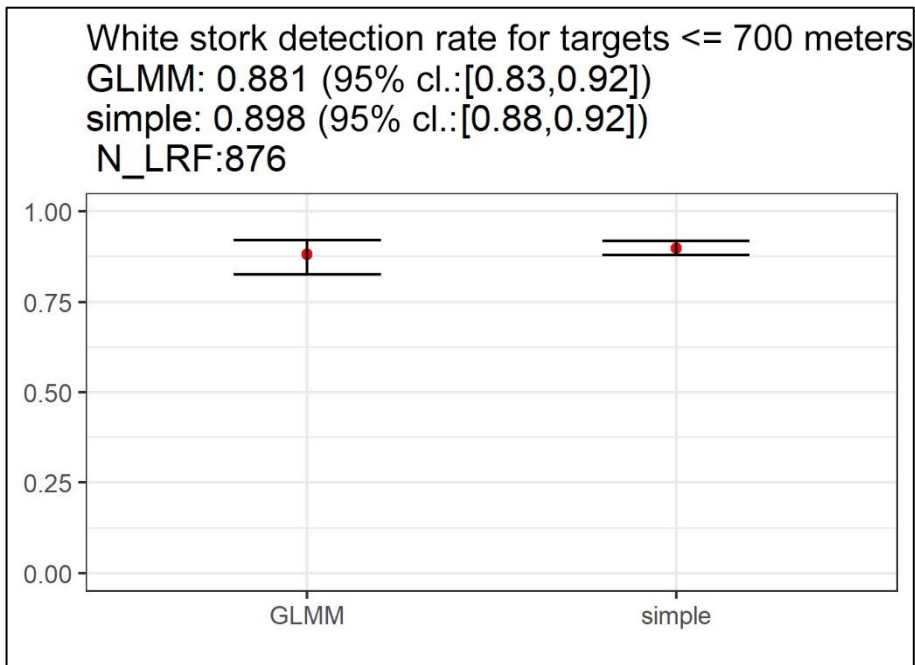

Fig. A.8: Statistical results of the white stork detection rate. GLMM analyses (left) vs. the "simple" approach (right) based on a detection radius of 700 m (≥ the response radius up to max. 700 m). Red dots indicate mean values, black bars 95% confidence intervals. N_LRF indicates the number of underlying LRF points.